

YORICK A. BIRKHÖLZER

NANOMECHANICAL SENSING OF
HYPERMETHYLATED DNA FOR THE
DETECTION OF BLADDER CANCER

MESA+
INSTITUTE FOR NANOTECHNOLOGY

**UNIVERSITY
OF TWENTE.**

BACHELOR OF SCIENCE THESIS

Advanced Technology
Inorganic Materials Science
2015

BACHELOR ASSIGNMENT COMMITTEE

Chairman Prof. dr. Guus Rijnders
Supervisor Dr. Ruud Steenwelle
External member Dr. Herbert Wormeester

CHAIR

Inorganic Materials Science
Faculty of Science and Technology
University of Twente

Yorick A. Birkhölzer: *Nanomechanical sensing of hypermethylated DNA for the detection of bladder cancer*, Bachelor of Science thesis, © 2015.

E-MAIL:
yorick.birkholzer@gmail.com

ABSTRACT

This thesis explores a novel nanomechanical DNA sensor that is being developed for the detection of bladder cancer. The proposed device comprises an array of microcantilevers, whose resonance frequencies change upon molecular adsorption. This shift in resonance frequency is the working principle of the novel device. Laser Doppler vibrometry is used to measure the resonance frequency of the thermally actuated cantilevers. By functionalizing the cantilever surface with thiolated single-stranded DNA, the cantilever sensor is made sequence-specific for the hybridization of complementary DNA strands. New devices are fabricated and characterized by ellipsometry, scanning electron microscopy and electron dispersive X-ray spectroscopy. Surface functionalization is studied with fluorescence microscopy and X-ray photoelectron spectroscopy. A DNA concentration of $1\ \mu\text{M}$ in TE-buffer is readily detected and distinguished from non-specific adsorption. The sensor performance is drastically improved by reducing non-specific interactions via backfilling with a PEG-Silane anti-fouling agent prior to DNA hybridization. Current theoretical models for mass, stress, and stiffness effects on cantilever resonance frequencies are numerically evaluated but cannot explain the large magnitude of sensor response found experimentally.

ACKNOWLEDGEMENTS

I'd like to thank my supervisor Ruud for his daily guidance, chairman Guus for keeping track of the bigger picture, and my office mate Harmen, who started a few months before me on this project and did a great job working me in. We performed many of the experiments described in this thesis together. Special thanks goes to Özlem who enabled multiple visits to the cleanroom and let me experience the full fabrication process of the devices I later on performed my experiments on. Many thanks to Roberto and Raquel for performing the synthesis in the chemical lab together with me. Thanks to Herbert for serving as external member of the committee and providing valuable feedback in the early phase when I had just chosen this assignment. Besides, our work at the synchrotron in Grenoble was very inspiring, giving me a great impression of fundamental surface science. Finally, thanks to my friends and family who supported me during my entire Bachelor phase in the Netherlands, especially those who helped me proofreading this thesis.

CONTENTS

1	INTRODUCTION	1
1.1	Fundamentals	1
1.1.1	DNA sensing	1
1.1.2	Cantilever sensors	2
1.2	Embedding of a novel DNA sensor	2
1.2.1	Background	2
1.2.2	Market	3
1.2.3	Ethics	3
1.3	Aims and approach	4
2	THEORY	5
2.1	Mechanics	5
2.2	Designs	6
2.3	Resonance frequency	7
2.3.1	Analytic computation	7
2.3.2	Finite Element Method	7
2.4	Shift of the resonance frequency peak	8
2.4.1	Mass effect	9
2.4.2	Stress effect	9
2.4.3	Stiffness effect	9
2.5	Thermal actuation and noise	10
2.6	Surface functionalization	11
2.7	Anti-fouling	11
2.8	Discussion & conclusion	12
3	FABRICATION	13
3.1	Dry etching and isotropic wet etching	13
3.2	Gold deposition	15
3.3	Anisotropic wet etching	15
3.4	Discussion & conclusion	16
4	EXPERIMENTAL WORK	17
4.1	Sample preparation	17
4.2	Round 1	17
4.3	Round 2	18
4.4	Round 3	18
4.5	Laser Doppler vibrometry	19
4.6	Scanning electron microscopy and energy dispersive X-ray spectroscopy	20
4.7	X-ray photoelectron spectroscopy	20
4.8	Fluorescence microscopy	21
4.9	Surface plasmon resonance	21
4.10	Discussion & conclusion	21
5	RESULTS	23
5.1	Round 1	23
5.2	Round 2	24
5.3	Round 3	26

5.4	Surface Plasmon Resonance	26
5.5	Silicon oxide devices	28
5.6	Time effect of the TE - buffer	28
6	DISCUSSION & RECOMMENDATIONS	31
6.1	Experimental round 1	31
6.2	Experimental round 2	31
6.3	Experimental round 3	32
6.4	Applicability of the theoretical model	33
6.5	Recommendations for further research	34
7	CONCLUSION	35
A	APPENDIX	37
A.1	Flexural vibrations of a cantilever	37
A.2	Low aspect ratio of the cantilever	39
A.3	Mass effect	40
A.4	Stiffness effect	40
A.5	Aluminum debris	41
A.6	Challenges	44
A.7	Additional fluorescence microscopy images	45
A.8	Additional XPS data	45
	BIBLIOGRAPHY	47

ABBREVIATIONS & SYMBOLS

α	Eigenvalue
A	Cross-sectional area
b	Width of the cantilever
δ_{rms}	Root mean square tip deflection
E	Young's modulus
f	Resonance frequency
Δf	Change in resonance frequency
h	Height of the cantilever
K	Spring constant
k_B	Boltzmann constant
L	Length of the cantilever
m	Mass
ν	Poisson's ratio
I	Second moment of area
ρ	Density
σ	Surface stress
T	Temperature
BHF	Buffered hydrofluoric acid
CpG	Cytosine and guanine nucleotide separated by a phosphate
DNA	Deoxyribonucleic acid
EDS	Energy dispersive X-ray spectroscopy
FEM	Finite element method
FFT	Fast Fourier transform
LDV	Laser Doppler vibrometer
LPCVD	Low pressure chemical vapour deposition
MBD	Methyl binding domain
MUHEG	Mercaptoundecyl hexaethylene glycol (C ₂₃ H ₄₈ O ₇ S)
NEMS	Nanoelectromechanical system
OEG	Oligoethylene glycol
PEG	Polyethylene glycol
PZT	Lead zirconate titanate
RIE	Reactive ion etching
SAM	Self-assembled monolayers
SEM	Scanning electron microscope
Si ₃ N ₄	Silicon nitride
SiO ₂	Silicon oxide
ssDNA	Single-strand DNA
SPR	Surface plasmon resonance
TMAH	Tetramethylammoniumhydroxide
XPS	X-ray photoelectron spectroscopy
3'	3 Prime end of a DNA strand
5'	5 Prime end of a DNA strand

1 | INTRODUCTION

Bladder cancer is the fifth most common cancer in the western world [Kandimalla et al., 2013]. For decades, extensive research on biosensors has been performed since, in general, cancer treatment is more effective the earlier the disease is detected. One possible route for the detection of bladder cancer, nanomechanical sensing of hypermethylated DNA in urine, is investigated in this Bachelor thesis.

Biosensors are devices that couple a biological recognition element with a physical transducer that translates the bio-recognition event into a measurable effect, such as an electrical signal, an optical emission or a mechanical motion. Biosensors based on cantilevers are a good example where nanotechnology and biotechnology come together as microcantilevers translate recognition of biomolecules into nanomechanical motion.

Hypermethylated DNA in urine is a biomarker for bladder cancer

The small size and high sensitivity of nanomechanical resonators enable the use of arrays of uniquely functionalised cantilevers in a miniaturized sensor device. Nanoelectromechanical systems (NEMS) allow selective, multiplexed, label-free molecular recognition through these arrays and improved reliability through on-chip redundancy for each analyte [Waggoner et al., 2009].

1.1 FUNDAMENTALS

1.1.1 DNA sensing

There are several differences in the DNA of cancer cells and normal cells. Scientists are developing tests that identify these DNA changes in order to diagnose cancer. Currently much research is conducted on the detection of bladder cancer in urine [Xylinas et al., 2014]. It has been shown that DNA methylation contributes to the development of various cancers including bladder cancer [Kandimalla et al., 2013]. Besides the medical field, detection of DNA has potential applications in food safety, forensic science and counter-terrorism [Ferrier et al., 2015].

DNA methylation does not alter the genomic DNA sequence itself, but covalently bonds methyl (CH₃) groups on cytosines of cytosine-phosphate-guanine (CpG) dinucleotides [Delpu et al., 2013; Hoque et al., 2006]. CpG rich regions known as CpG islands, which span the 5' end region of many genes, are usually unmethylated in normal cells. These genes can be transcribed regularly. In cancer cells, however, hypermethylation leads to transcriptional inactivation and is a major mechanism for silencing tumor suppressor genes [Esteller, 2007]. A large number of DNA methylation-based biomarkers has been reported that principally involve hypermethylation of tumor suppressor CpG islands. The naturally occurring methyl binding domain (MBD) proteins are known to bind to

DNA hypermethylation refers to the gain of methyl groups at specific sites that are unmethylated under normal conditions.

methylated CpG dinucleotides and subsequently recruit other proteins to suppress transcription [Yu et al., 2010].

1.1.2 Cantilever sensors

The resonance frequency of a cantilever changes when biomolecules adsorb on it

Due to advances in micro- and nanofabrication it is possible today to fabricate nanosized mechanical transducers with vibrating parts whose resonance frequencies are sensitive to molecular adsorption. As the sensitivity is inversely proportional to the active mass of the resonator, a smaller sensor promises lower detection limits. The basic principle of the nanomechanical sensor in this project is the measurement of the resonance frequency shift, e.g. caused by the added mass of the molecules bound to the cantilever surface. When a biomolecule adsorbs on the suspended mechanical structure, not only the mass changes, but also surface stress, the effective Young's modulus and viscoelasticity are influenced. This type of sensor works label-free, meaning that targeted molecules are not labeled or altered but directly detected in their natural form [Tamayo et al., 2013].

Ramos et al. [2009] observed that the influence of an adsorbed bilayer at the cantilever basis on nanoscale elasticity gives a stronger (positive) shift of the resonance frequency than the classically predicted and measured mass effect at the cantilever tip. The mass effect causes a decrease in resonance frequency, whereas increasing stiffness highers the resonance frequency. According to Eom et al. [2011], surface effects only play a significant role when the thickness of the nanocantilever becomes smaller than 100 nm.

1.2 EMBEDDING OF A NOVEL DNA SENSOR

1.2.1 Background

Cystoscopy is invasive and relatively expensive

Patients with bladder cancer are monitored for cancer recurrence or progression by periodic cystoscopy and urine cytology every 3-12 months [Kandimalla et al., 2013]. Urine cytology is a test to look for abnormal cells in urine by examining cells under a microscope. Cystoscopy is a form of endoscopy, where a doctor examines the urinary bladder via the urethra, the tube through which urine leaves the bladder towards the outside of the human body. Studies on the efficacy of cystoscopy reveal that tumors are missed in 10-40 % of patients [Kelly et al., 2012].

Future applications of DNA sensors require technology that enables point-of-care treatment or on-site testing with no need for centralized laboratories and specialized personnel. Therefore, sensors must be simple, low-cost, portable and rapid; work with small volumes of sample material and be sufficiently sensitive and specific with dynamic range for the intended purpose. Nanoelectromechanical DNA sensors work label-free which makes their sensing mechanisms much simpler than most electrochemical or optical techniques in terms of steps involved and reagents required [Ferrier et al., 2015].

Ultimate goal of micro- and nano-cantilever sensors is the use of large-scale arrays to enable biomolecular fingerprinting, a *nanomechanical nose* that can detect multiple analytes simultaneously, e.g. lung cancer markers in exhaled

breath. In the *Nanopill 2.0* project at the University of Twente, a microfluidic platform for early cancer diagnostics is being developed. Eventually, a patient can swallow a sensor in form of a pill that can detect cancer markers while the pill travels through the patient's intestines and inform the physician through wireless communication. Also within the framework of this *Nanopill 2.0* project, a nanomechanical cantilever sensor for the detection of bladder cancer via hypermethylated DNA in urine is being developed and that is the focus of this thesis.

1.2.2 Market

Nanoelectromechanical systems can be integrated into lab-on-a-chip systems to perform portable point-of-care analysis. Advantages of NEMS are robustness, reliability, and low energy consumption [Carrascosa et al., 2006]. The use of well-established semiconductor technology allows for the batch production of arrays of hundreds of NEMS with consequent cost reduction of mass production. The global market for MEMS bio- and nanosensors is estimated to be \$15.8 billion in 2018. [McWilliams, 2013]

Microelectronics industry reduces costs via economies of scale

Bladder cancer has the highest lifetime treatment costs per patient of all types of cancer. Sievert et al. [2009] conclude in their study of the economical aspects of bladder cancer that urine-based tests have significant potential to improve diagnosis and monitoring of patients with potential improvements in clinical outcomes and concurrent cost-savings. Svatek et al. [2014] state that urine-based markers are more sensitive than cytology, albeit being less specific, and can help reducing the use of cystoscopy, which is the most sensitive but rather expensive method to detect bladder cancer. They conclude that further refinement of urine-based markers is still necessary to achieve a truly noninvasive test for bladder cancer.

1.2.3 Ethics

All-encompassing cancer screening is not uncontroversial. A case comparable to bladder cancer but better discussed in literature is prostate cancer. Since the 1990s, routine screening for prostate cancer is done by testing for prostate-specific antigen (PSA), a biomarker associated with prostate cancer. The problem with this screening is summarized in an article published by The Wall Street Journal that quotes Dr. Richard Ablin, the person who discovered PSA in 1970: The PSA test cannot distinguish an indolent cancer from an aggressive one [Beck, 2013]. According to this article, up to 80 % of man aged above 75 possess asymptomatic cancer. The problem is that too many men are unnecessarily treated for cancers that will ultimately prove to be of little harm. While some cancers are fast-moving and lethal, many others grow so slowly that they don't cause any problems.

Screening is looking for cancer before a person has symptoms

Every single person, even those who we perceive as completely healthy, has some kind of anomaly. On the genetic level, nobody will ever be perfect [LeBlond, 2012]. The virtually ideal person, free of any disease or whatsoever, does not exist [Xue et al., 2012]. Yet, that doesn't mean that we are all sick. Not knowing about one's imperfections might actually be a relief rather than a threat. It is doubtful that we would be happier if we knew everything there is to measure on and in our body. But where should we draw the line? What should the threshold

values of future sensors be? These questions are not easy to answer and require solid reflections by an ethic council, where medical experts, physicists, biologists, and engineers come together.

Early detection of cancer saves lives

Concluding, medical and psychological side effects might be reasonable cause that make us hesitate to screen for cancer in the broadest, technologically feasible sense. However, despite all criticism, cancer screening and early detection have saved thousands of lives [Fradet, 2009]. Until the nanomechanical sensor, which this thesis is about, is ready for commercial, clinical application, there is still a number of technical obstacles to be overcome.

1.3 AIMS AND APPROACH

This Bachelor thesis has a focus on experimental work

Recent experiments of the *Inorganic Materials Science* (IMS) group on their nanomechanical cantilever sensors have generated mixed results such as unrealistic magnitude and varying response of parallel experiments. A range of effects are expected to play a role, such as humidity of the environment, concentration of the analyte, sensor geometry, functionalization geometry, and non-specific interactions such as the deactivation of the self-assembled monolayer (SAM) by the non-complementary DNA control step. The purpose of this project is to carry out a set of experiments that shed more light on the involved interactions influencing the sensing process.

First and foremost, the chemical functionalization sequence is investigated. In step one, thiol-terminated single-stranded DNA (ssDNA) probes are immobilized on a gold surface, and in step two, these probes are hybridized with complementary DNA target strands and non-complementary control. The goal is to functionalize a cantilever in such a way that by only measuring the shift of its resonance frequency, hybridization with complementary DNA can be distinguished from non-specific adsorption and non-complementary DNA. This, in principle, allows for sequence specific DNA detection. Surface plasmon resonance (SPR) is used as an established reference technique for DNA hybridization measurements. Fluorescent labeling is used to verify the areal density of the DNA molecules. Scanning electron microscopy (SEM) and energy dispersive X-ray spectroscopy (EDS) are used for imaging and elemental analysis. X-ray photoelectron spectroscopy (XPS) is used as a surface sensitive characterization technique. Cantilever resonance frequencies are measured by laser Doppler vibrometry (LDV). The fabrication of the new microcantilever devices is followed as a guest in the cleanroom.

This project, detecting bladder cancer via nanomechanical sensing of hypermethylated DNA, combines various disciplines such as materials science, physics, biomedicine, chemistry, and mechanics and therefore suits a true *Advanced Technology* attitude. To my best knowledge, no paper has yet been published on the detection of bladder cancer via nanomechanical sensing of hypermethylated DNA, which makes my Bachelor assignment unique and exciting.

This thesis is structured as follows: In chapter 2, the theory is explained, followed by a description of the device fabrication in chapter 3. In chapter 4, techniques and experimental work are described. The results are presented in chapter 5 and discussed in chapter 6. The conclusions are given in chapter 7.

2 | THEORY

The goal of the sensor studied in this thesis is the detection of bladder cancer via nanomechanical sensing of hypermethylated DNA. The detection mechanism used in this type of sensor relies on the shift of resonance frequency of a microcantilever upon specific adsorption of certain biomarkers. This chapter establishes the necessary theory to develop a model that allows for a prediction of the resonance frequency shift to be expected in the experiments. First an analytic description is given for a simplified geometry, followed by a more sophisticated, numerical model created with the finite element method software package COMSOL, which resembles the real design of the cantilever sensor more closely.

2.1 MECHANICS

The theory of flexural vibrations of beams is derived and explained in many textbooks on solid mechanics [Magrab, 2012; Strømmen, 2014]. An excellent review on biosensors based on nanomechanical systems is given by Tamayo et al. [2013]. Another recommendable, but slightly older review is written by Eom et al. [2011] on the nanomechanics principles for nanomechanical resonators and their applications in biological and chemical detection.

Cantilevers are mechanical structures consisting of a beam anchored only at one end and being free at the other, schematically shown in fig. 1. In the resonant, or dynamic, mode, the cantilever beam is brought into oscillation, here via electric actuation of a lead zirconate titanate (PZT) layer, a material with a high piezoelectric coefficient. Thermal energy at room temperature already causes the cantilevers to oscillate. In some experiments, this is regarded as detrimental noise, but in other circumstances this fundamental property can also be used deliberately for thermal actuation as shown in section 2.5.

For this thesis project, novel devices made of silicon oxide (SiO_2) and silicon nitride (Si_3N_4) without a piezoelectric actuation layer were fabricated. Their dimensions and properties are summarized in table 1. This chapter focuses on the properties of these new devices as they have been used for all functionalization experiments. Different types of cantilevers are introduced. First their design is explained, second their resonance frequency is computed, and third an estimation for the expected frequency shift upon molecular adsorption is made.

Two different types of cantilevers are used in this thesis, referred to as SiO_2 and Si_3N_4

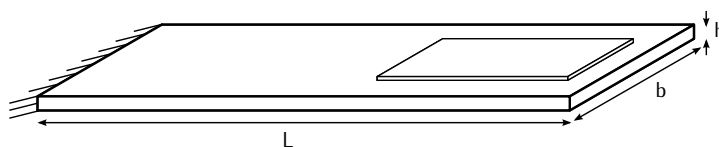


Figure 1: Cantilever beam with a patch at the tip, fixed end on the left and free end on the right.

Table 1: Dimensions and properties of the cantilevers, thickness h , density ρ , Young's modulus E , and Poisson's ratio ν . Both types of cantilevers have a length $L = 200 \mu\text{m}$ and width $b = 100 \mu\text{m}$; the indicated thickness is the height of the beam without the thickness of the additional gold patch.

Type	h (μm)	ρ (kg m^{-3})	E (GPa)	ν
SiO_2	0.834	2650	70	0.17
Si_3N_4	0.519	3100	210	0.23

This theory chapter then continues with sections on thermal actuation and chemical surface functionalization.

2.2 DESIGNS

There are multiple device designs on the fabricated wafers

The wafers that were fabricated comprise three essential designs: cantilevers, paddles, and bridges. Classical cantilevers as shown on the left in fig. 2 are of foremost importance in this thesis. Paddles differ from normal cantilevers by having a much wider tip than base, see fig. 2 (middle). Lastly, bridges are beams that are clamped at both ends, represented in fig. 2 on the right. In section 2.3 the resonance frequency of these devices is calculated. The fabrication of these devices is described in chapter 3.

Side note: For the *Nanopill 2.0* project multi-layered cantilevers with a built-in piezoelectric layer for actuation and read-out were actually to be used. However, unpublished experiments by Harmen Koster, a colleague Bachelor student, revealed major problems of this design just in the 1st week of this thesis project. Main problems were electrostatic attraction of DNA by uncovered PZT and gold patches peeling off the cantilever surface, a summary of the problems with the original cantilevers is given in appendix A.6. Future wafers are produced using improved lithography masks and different adhesion layers under the gold. Fabrication of these multi-layered cantilevers is a complex process and not feasible in the given time frame. That is why simpler, alternative devices were used.

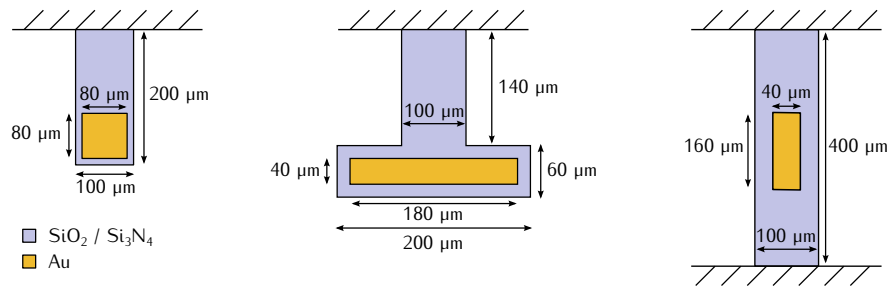


Figure 2: Schematic drawing of the cantilever, paddle, and bridge microdevice designs.

2.3 RESONANCE FREQUENCY

2.3.1 Analytic computation

The multi-layered architecture of the cantilevers used in the *Nanopill 2.0* project lacks the necessary symmetry for an exact analytical expression for its resonance frequency. Therefore, a simplified model of a 1 dimensional cantilever beam is used as a first approximation. For convenience, a summary of the derivation is given in appendix A.1.

The resonant or natural frequency of the flexural modes is given by,

$$f_n \approx \frac{\beta_n^2}{21.7656} \sqrt{\frac{E}{\rho}} \frac{h}{L^2} \quad (1)$$

where E is the Young's modulus, ρ the material density, h the beam thickness, L the beam length, and β_n the eigenvalue. Table 2 shows a comparison of the lowest order resonant frequency, thus for an eigenvalue $\beta_1 = 1.85710$. The analytical expression applies for the reference cantilevers without a gold patch. In table 2, the resonance frequencies of cantilevers with and without gold are compared

The cantilevers used for the experiments described in this thesis have a low length to width aspect ratio. This raises the question whether Euler-Bernoulli beam theory, which was derived for long, slender beams, is still applicable. [Looker and Sader \[2008\]](#) derived an analytical expression for flexural resonant frequencies of thin, rectangular, 2-dimensional cantilever plates. Their model allows for small, finite L/b aspect ratios, which Euler-Bernoulli beam theory does not. For the cantilever geometry used here, the difference in resonant frequency between the 1-dimensional Euler-Bernoulli beam model and the cantilever plate model derived by [Looker and Sader \[2008\]](#) is less than 2%. See appendix appendix A.2 for the full calculation.

Applicability of 1-D Euler-Bernoulli beam model is verified with 2-D cantilever plate model

2.3.2 Finite Element Method

The finite element method software package COMSOL is used to discretize the exact cantilever geometry with a very fine swept mesh containing 30000 quadrilateral elements. The *Solid Mechanics* package of COMSOL is used to perform an *Eigenfrequency* analysis. The resonance frequencies obtained with

Table 2: Resonance frequencies of the cantilevers with gold patch (FEM model) and without gold patch (analytical model).

Model	Gold patch	Model	Resonance frequency (Hz)
SiO ₂	no	Analytical	16980
SiO ₂	no	FEM	17450
SiO ₂	yes	FEM	13784
Si ₃ N ₄	no	Analytical	16921
Si ₃ N ₄	no	FEM	17507
Si ₃ N ₄	yes	FEM	13045

Eigenfrequency $f = 13045$ Hz
 Surface: total displacement (arb. unit)

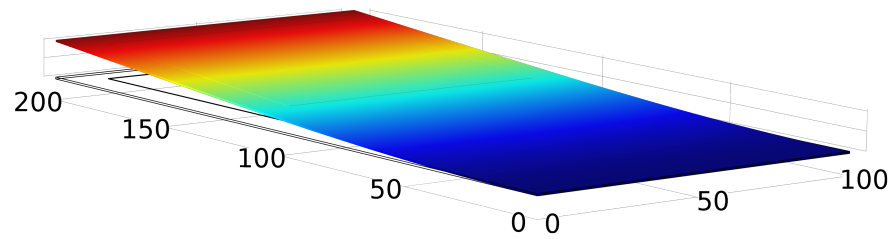


Figure 3: Simulation result of the eigenfrequency analysis for a Si_3N_4 cantilever. Image shows the deformation shape of the first flexural mode, dimensions in μm and displacement in arb. unit.

FEM results are in agreement with analytical approximation

this FEM model for the cantilevers with and without gold patch are shown in table 2. Only the first, fundamental mode is given since this is the only one of interest for the experiments later on. Higher order modes have less vibrational amplitude and are therefore more difficult to measure. The results of this finite element analysis show resonance frequency for the cantilevers without a gold patch that is about 3 % higher compared to the values computed analytically with the 1-D Euler-Bernoulli beam model. This is considered a good agreement in the given context. As indicated in the previous section, the error of the Euler-Bernoulli model is due to the low length to width aspect ratio of the cantilevers used here, which the Euler-Bernoulli model was not derived for. The 2-D cantilever plate model by [Looker and Sader \[2008\]](#) naturally performs much better in such a situation and is even found to be within 1 % agreement with the FEM results.

The result of the COMSOL simulation, the deflection shape of the first flexural mode result and the corresponding eigenfrequency are shown in fig. 3, which is qualitatively representative for both silicon oxide and silicon nitride cantilevers. Note that the amplitude of the deflection in the eigenfrequency analysis (fig. 3) is intrinsically arbitrary and doesn't carry quantitative information. In section 2.5, however, realistic amplitudes of tip deflection are computed for thermal actuation at room temperature.

2.4 SHIFT OF THE RESONANCE FREQUENCY PEAK

Changes in mass, surface stress, and stiffness of a cantilever are the main contributions to the shift of the resonance frequency

The resonance frequency of a cantilever changes upon molecular adsorption. This effect is assigned to alterations in three main variables of the cantilever, namely mass, surface stress, and stiffness of the cantilever. For each of these three parameters that contribute to the total shift of the resonance frequency there exist separate models in literature that try to predict the respective effect on the resonance frequency. Depending on the sensor geometry and the analytes of interest, the magnitude of the individual contributions can vary by several orders of magnitude [[Tamayo et al., 2013](#)]. All three analytical models, the mass, stress, and stiffness effect, have to be used with caution. They are derived under many assumptions and only meant to serve as a fast tool to estimate the order of magnitude of a cantilever sensor response. There are far more experimental variables that are not captured by these models and therefore the exact behavior of a cantilever sensor cannot possibly be predicted by these models.

2.4.1 Mass effect

The most prominent explanation for the frequency shift of a cantilever is based on the added mass of the atoms adsorbing on the cantilever surface. The mass sensitivity of a cantilever beam is highest at its tip and that is why the gold patches of the cantilevers used are placed there. The relative change in resonance frequency due to adsorbed mass on a cantilever beam can be approximated by the following relation,

$$\frac{\Delta f}{f_0} \approx -\frac{1}{2} \frac{m_a}{m_b} \quad (2)$$

Here Δf denotes the absolute shift of the resonance frequency f_0 due to added mass on the cantilever. m_a and m_b are the mass of the adsorbate layer and the beam, respectively. Making a reasonable estimate for m_a and m_b , a relative frequency shift of $\sim -0.005\%$ is expected from the mass effect according to this simple model. This corresponds to an expected measurable frequency shift of about -1 Hz. The full calculation is given in appendix A.3. The well-known quartz crystal microbalances (QCM) also use the fact that an increase in mass causes a decrease in resonance frequency.

Mass effect is small

2.4.2 Stress effect

Surface Stress is the amount of reversible work per unit area needed to elastically stretch a pre-existing surface. Adsorption on a surface can generate changes in the surface stress as a consequence of the adsorbate-surface and adsorbate-adsorbate interactions. Electrostatic force, hydration force, viscoelasticity, and conformational entropy are exemplary contributions to surface stress [Doínguez et al., 2014; Mertens et al., 2008; Yang, 2012]. A linear model for the effect of changing surface stress on the resonance frequency of a cantilever beam due to adsorption is given by Tamayo et al. [2013] as

$$\frac{\Delta f}{f_0} \approx \frac{1-\nu}{Eh} \left[-0.042\nu \frac{b^3}{Lh^2} + \frac{1+2\nu}{1-\nu} \right] (\sigma_u + \sigma_b) \quad (3)$$

where E is the Young's modulus of the cantilever material, L , b , h are the cantilever length, width, and height, respectively, ν denotes the Poisson's ratio, and σ_u and σ_b are the surface stress in the upper and bottom sides of the beam. Substituting the data of the cantilevers used in the experiments of this thesis, one obtains a relative frequency change at the order of just a few ppm, which is far below the noise level of the measurements taken. This result agrees with an article by Xu and Deng [2013], who state that surface effects only play a significant role when the thickness of the beam is lower than hundred nanometers, which is clearly not the case for the cantilevers used here.

Surface stress effect is negligible for the cantilevers used in this thesis

2.4.3 Stiffness effect

Adsorption of molecules does not only increase the total effective mass of a cantilever, but an adlayer also has a certain stiffness. The resonance frequency shift due to homogeneous adsorption with an effective layer of thickness h_a formed on the cantilever beam is given by Tamayo et al. [2013] as

$$\frac{\Delta f}{f_0} \approx \left(\frac{3E_a}{2E_b} - \frac{\rho_a}{2\rho_b} \right) \frac{h_a}{h_b} + \frac{3}{8} \left[\left(\frac{\rho_a}{\rho_b} \right)^2 - 3 \left(\frac{E_a}{E_b} \right)^2 - 2 \frac{E_a \rho_a}{E_b \rho_b} \right] \left(\frac{h_a}{h_b} \right)^2 \quad (4)$$

Stiffness effect is expected to be dominant

where subscript a and b denote properties of the adsorbate layer and the beam, respectively. For the cantilevers studied in this thesis, the model overestimates the stiffness effect as it assumes homogeneous adsorption over the whole surface area of the cantilever. The experiments, however, are designed such that DNA probes – in ideal case – are only immobilized on the gold patch at the cantilever tip by means of metal-thiolate bonding. Besides this geometric confinement, stiffness responsivity is known to decrease from the cantilever base to the tip [Tamayo et al., 2013]. Despite these two limitations, the model is evaluated for the cantilevers used in this project. A relative resonance frequency shift of -0.5% is calculated, which contradicts with the intuitive reasoning that an adlayer would increase the effective stiffness of a cantilever and thereby increase the resonance frequency. It may be noted that the effective Young's modulus of a DNA monolayer has to be estimated as there are no values reported in literature. The full calculation is given in appendix A.4. The model is particularly sensitive to the Young's modulus of the adlayer, which is, unfortunately, the hardest parameter to determine experimentally in this context. For large values of E_a approaching E_b , the calculated frequency shift can also become $+2\%$. Again, not the exact number is of importance, but what matters is the order of magnitude.

Summarizing, the surface stress effect is expected to be negligible and the stiffness effect is calculated to be $100\times$ larger than the mass effect. Therefore, the stiffness effect is expected to be the major contributor to the frequency shift upon DNA hybridization.

2.5 THERMAL ACTUATION AND NOISE

Si₃N₄ cantilevers without piezoelectric layer have to be actuated thermally

The silicon nitride cantilevers used do not have a built in PZT layer for piezoelectric actuation. They have to be analyzed under thermal actuation. From the equipartition theorem,

$$\frac{1}{2}K\delta_{\text{rms}}^2 = \frac{1}{2}k_B T \quad (5)$$

it can be deduced that the root mean square tip deflection is

$$\delta_{\text{rms}} = \sqrt{\frac{k_B T}{K}} \quad (6)$$

where k_B is the Boltzmann constant, T the temperature of the cantilever and K its effective spring constant. For a cantilever beam, the spring constant is given by

$$K = \frac{Ebh^3}{4L^3} \quad (7)$$

where E is the Young's modulus and b , h , L are the width, height, and length of the cantilever, respectively. This simple model is evaluated for the dimensions and properties of the cantilevers used in this thesis (see table 1) and the results are summarized in table 3. For comparison with previous generations of cantilevers used in the *Nanopill 2.0* project, a third and thicker type of cantilever made of pure silicon is added in that table. The tip deflection of the new devices due to thermal actuation, sometimes also called Brownian motion in this context, is about 200 pm. Although this is quite a low value, it is still measurable by laser Doppler vibrometry.

Table 3: Tip deflection due to thermal energy at room temperature ($T = 295\text{ K}$).

Type	Thickness h (nm)	Tip deflection δ_{rms} (nm)
Si_3N_4	519	0.21
SiO_2	834	0.18
Si	4000	0.01

2.6 SURFACE FUNCTIONALIZATION

For an inorganic microcantilever to obtain biosensing properties, its surface must be functionalized by applying a suitable surface chemistry routine. The goal of the proposed biosensor is the sequence-specific detection of DNA strands. Therefore, it is chosen here to capture these DNA targets with complementary single-stranded DNA probes, which are immobilized on the gold coated cantilever surface with thiol groups. Gold is chemically inert, but is accessible to chemisorption via thiolate bonding.

Proper surface functionalization turns an ordinary microcantilever into a biosensor

The performance of the functionalization strategy depends both on the surface density of target molecules as well as the blocking strategy to limit non-specific adsorption as much as possible. Surface coverages of ~ 0.1 molecules nm^{-2} are reported in literature [Álvarez et al., 2004; Herne and Tarlov, 1997; Keighley et al., 2008; Steel et al., 2000]. This value corresponds to a relative monolayer coverage of about 10%, which means that there is sufficient space for the target molecules to reach the immobilized ssDNA in the hybridization step. However, this also means that there is a lot of uncovered surface area which is prone to non-specific adsorption.

2.7 ANTI-FOULING

Fouling is the accumulation of unwanted material on solid surfaces and generally detracts the function of a device [Vidyasekar et al., 2012]. Non-specific adsorption on the cantilevers poses a major challenge as the sensor response is massively degraded by the wrong molecules adsorbing on the cantilever surface and thereby changing the resonance frequency of the cantilever uncontrolledly. A properly working sensor must not only be sensitive, but also sufficiently specific. Specificity can, for instance, be enhanced by blocking non-specific adsorption through application of suitable surface chemistry strategies. Polyethylene glycol (PEG) derivatives are known for their property to act as anti-fouling agents by forming surface-grafted polymer brushes which heavily reduce non-specific adsorption [Kosaka et al., 2013; Reimhult and Höök, 2015].

PEG-Silane has shown to function as a reliable anti-fouling agent on silicon nitride [Cerruti et al., 2008]. Silanes (SiH_4) have a low affinity to gold and preferentially bind to metal oxides [Reimhult and Höök, 2015]. Kosaka et al. [2013] presented promising results with backfilling of PEG-Silane on silicon and show that PEG outperforms other blocking agents such as bovine serum albumin. Backfilling in this context means that the cantilever surface area which is not covered by the probe molecules (here thiol-ssDNA) is filled with a dedicated substance deliberately after probe immobilization.

Backfilling with PEG-Silane is used to reduce non-specific adsorption



Figure 4: Skeletal formula of 11-mercaptoundecyl hexaethylene glycol, $C_{23}H_{48}O_7S$ (MUHEG).

Apart from protecting the non-gold areas from non-specific adsorption, back-filling is also used to increase the surface density of molecules on the gold itself. Therefore, short alkanethiols are used to fill up the space between the immobilized thiolated ssDNA. The increased surface density ensures that the ssDNA molecules stand in an upright position and do not hang down and stick to the gold surface. Mercaptohexanol $C_6H_{14}OS$ (MCH) is often used for this purpose [Adjémian et al., 2010; Li et al., 2014; Wernette et al., 2007]. Unpublished results by Alejandro Méndez Ardoy recently showed positive results when backfilling ssDNA layers on gold with 11-mercaptoundecyl hexaethylene glycol $C_{23}H_{48}O_7S$ (MUHEG), a neutral and flexible thiol terminated with hexaethylene glycol. MUHEG is used to resist nonspecific adsorption of biomolecules and polymers. The skeletal formula of MUHEG is shown in fig. 4.

2.8 DISCUSSION & CONCLUSION

In this chapter, a model for the expected shift in the cantilever resonance frequency was derived. Starting from basic solid mechanics, an analytical expression for the cantilever resonance frequency is given using Euler-Bernoulli beam theory as a first estimate. A FEM model is used to capture the dimensions and properties of the microcantilevers with gold patch more closely. Three complementary sub-models are discussed that each describe one contribution to the total resonance frequency shift upon molecular adsorption. These are the mass, stress, and stiffness effect. The latter is calculated to be most dominant. Furthermore, the chosen surface functionalization route, that turns an ordinary microcantilever into a biosensor, is explained with special attention to a chemical anti-biofouling strategy. Together, this forms the necessary theoretical background for the experimental part of this thesis.

3 | FABRICATION

This chapter describes the fabrication of silicon oxide and silicon nitride microcantilever devices. The process steps described in this chapter have been performed and explained by dr. Özlem Şardan Sukas, who kindly arranged a guest access to the cleanroom of the MESA+ Institute for Nanotechnology.

Fabrication of silicon oxide and silicon nitride microcantilever devices was followed in the MESA+ cleanroom

3.1 DRY ETCHING AND ISOTROPIC WET ETCHING

Starting material are four wafers (4-inch) of single-crystalline silicon (boron doped p-type Si (100), one-side polished). On two wafers, a thin film of thermal silicon oxide (SiO_2) is created by wet oxidation at 1100°C for 2 hours. On the other two wafers, a low-stress Si-rich silicon nitride (Si_3N_4) film is grown by low pressure chemical vapor deposition (LPCVD) for 2 h 5 min. The SiO_2 and Si_3N_4 layer thicknesses are measured by ellipsometry (Woollam M-2000UI) and found to be 834 nm and 519 nm, respectively.

Photoresist (positive resist, Olin OIR 907-17) is spin coated at 4000 rpm and pre-baked for 90 seconds minutes on a hotplate (90°C). Wafers and mask are carefully aligned and the photoresist is exposed to near UV light for 5 seconds in contact mode (EVC 620). Photoresist is developed for 45 seconds in a rough and fine bath of dedicated developing solution (Olin OPD 4262) and post-baked at 120° for 5 minutes (Si_3N_4) and 20 minutes (SiO_2). In the developing step, photoresist is removed such that the later cantilever features remain protected. Silicon nitride (Si_3N_4) wafers are dry etched in *TEtske*, a parallel plate reactive ion etch (RIE) system, using trifluoromethane CHF_3 plasma with a power of 60W for 12 minutes. Afterwards, photoresist is stripped with a 30 min oxygen plasma treatment (TePla 300). Silicon oxide wafers are cleaned by a short ozone treatment prior to wet etching in buffered hydrofluoric acid (BHF) for about 12 minutes and then rinsed with copious amounts of demineralized water. The ozone cleaning ensures that the etchant can efficiently reach the oxide by rendering the photoresist surface hydrophilic. Photoresist is removed in nitric acid (HNO_3).

Lithography with cantilever mask

Reactive ion etching (RIE) for Si_3N_4 wafer and BHF wet etching for SiO_2 wafer

In the next process step, photoresist is spin coated on the wafers again. This time a dynamic mode is chosen (up to 4000 rpm) such that the resist can spread well around and on the cantilever features. Baking, alignment, and exposure are performed analogue to the description above. In the developing step of this lithography process, photoresist is removed only from the places where gold has to be deposited in the next step, e.g. on the tips of many cantilevers.

Lithography with gold mask

For convenience, these first fabrication steps described so far are schematically represented in a simplified process diagram (fig. 5).

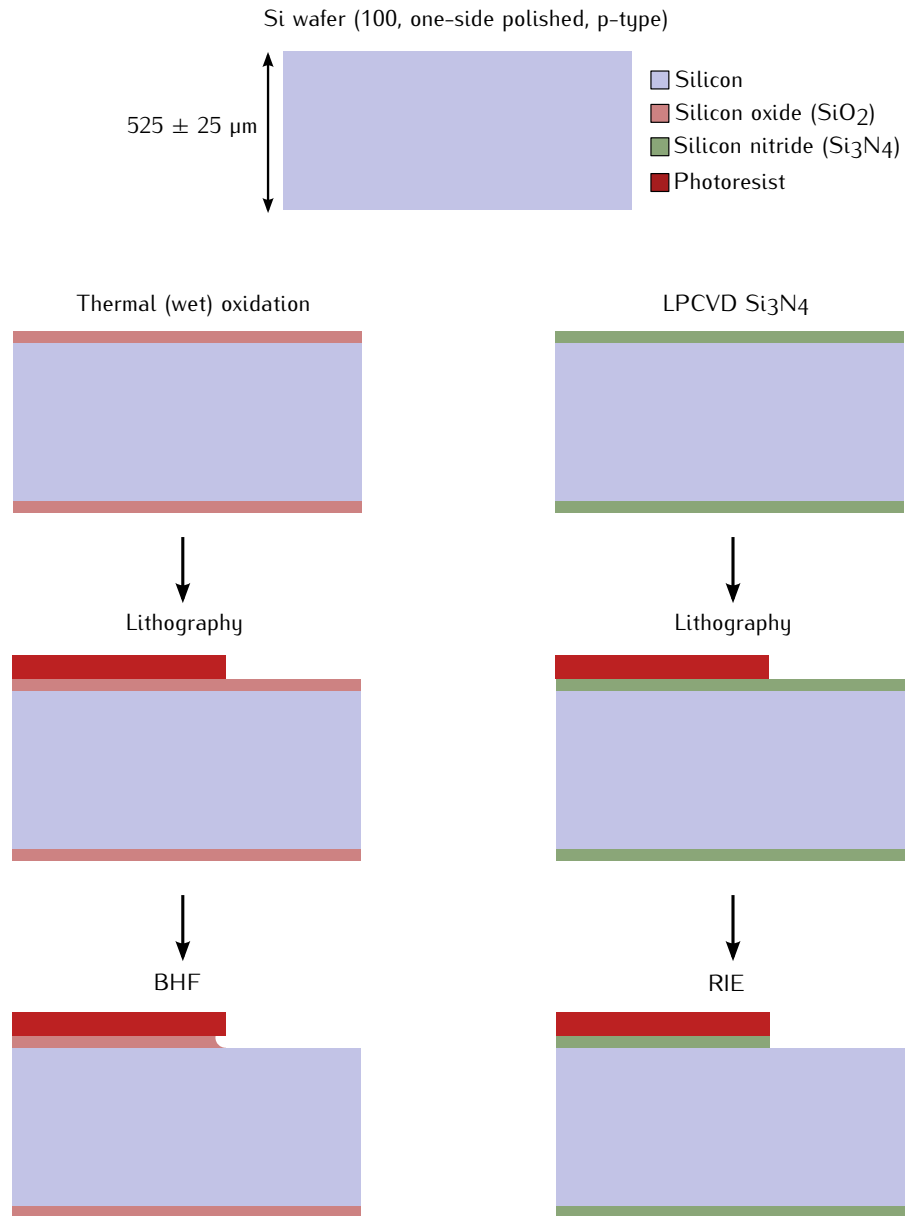


Figure 5: Schematic process diagram of the first 3 fabrication steps: thermal oxidation / LPCVD, Lithography, and reactive ion etching (RIE) / isotropic wet etching in buffered hydrofluoric acid (BHF).

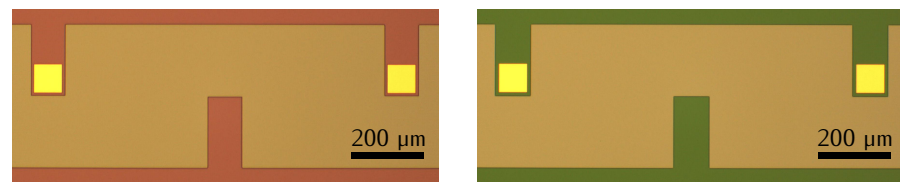


Figure 6: Unreleased silicon oxide (left) and silicon nitride (right) cantilevers with gold at the tip (top) and without gold (bottom) under an optical microscope (5× magnification). The colors are due to layer thickness and index of refraction. Real color images taken before anisotropic wet etching of the channel.

3.2 GOLD DEPOSITION

Deposition is performed with *Sputterke*, a single wafer sputter coater for deposition of metallic layers. First a 10 nm thin layer of titanium is sputtered to increase adhesion of the actual 100 nm gold layer, which is needed to functionalize the devices later on by means of thiol chemistry.

After the sputtering process, the entire upper wafer surface is covered with gold. The majority of this metallic layer lies on top of the photoresist and has to be removed such that only the desired features at the device tips remain covered with gold. This is done by lift-off in a beaker with acetone in an ultrasonic bath. After 15 minutes, the wafers are rinsed with isopropanol and demineralized water subsequently. Indeed, the sacrificial material is washed out and only the gold that was in contact with the underlying layer, the SiO_2 or Si_3N_4 wafer, respectively, remained. Integrity of the devices was verified under an optical microscope, see fig. 6.

Gold was deposited by sputtering and patterned by lift-off

The thickness of the cantilevers and the deposited layers is investigated by surface profilometry (Bruker Dektak 8). For the silicon nitride cantilevers, a height of 519 nm plus 115 nm titanium-gold was found, and for the silicon oxide cantilevers a height of 834 nm plus 120 nm. One of the SiO_2 wafers accidentally had double titanium deposition time (2 min instead of 1) and surface profilometry thereby also proves that the deposition rate of titanium in *Sputterke* is indeed 10 nm min^{-1} .

3.3 ANISOTROPIC WET ETCHING

Structures were released by anisotropic wet etching microfluidic channels (see fig. 7) in hot TMAH solution (tetramethylammoniumhydroxide, 85°C , 25 wt %) for about 2 hours. TMAH etches V-grooves in silicon with an angle of 54.74° between the $\langle 100 \rangle$ and $\langle 111 \rangle$ facets, thereby the cantilevers are underetched and thus released at the bottom side [Senturia, 2001].

Releasing the cantilevers by anisotropically etching the channels

Figure 8 shows a released Si_3N_4 cantilever with a gold patch at the tip. Figure 9 shows a bridge that is not properly released from the bottom of the microfluidic channel. Both chips are from the same wafer.

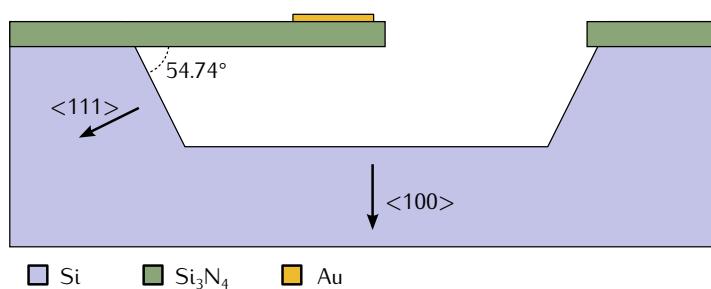


Figure 7: Schematic cross-sectional view of a silicon nitride cantilever in an anisotropically etched microfluidic channel.

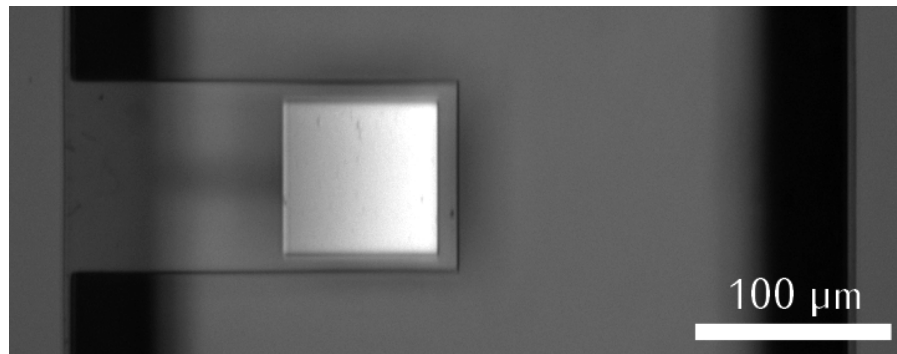


Figure 8: Released silicon nitride cantilever with gold patch at the tip. Greyscale image obtained with an optical microscope (10× magnification).

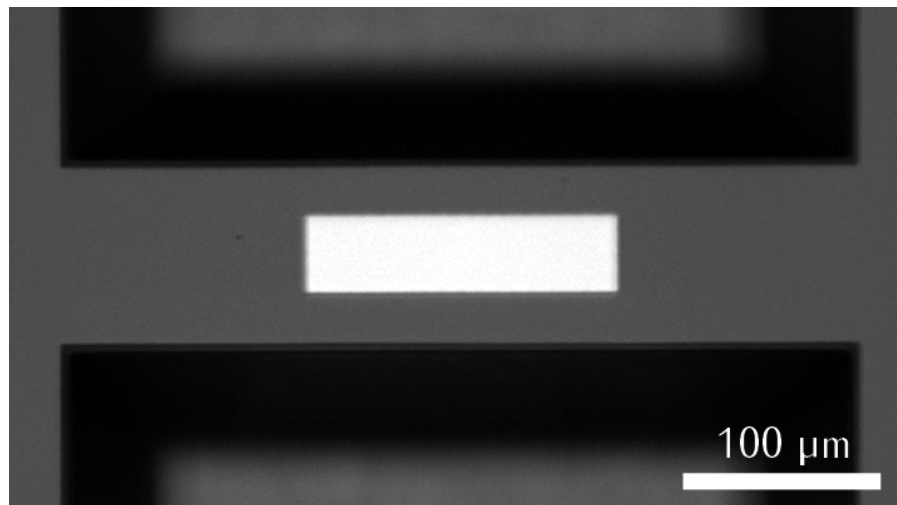


Figure 9: Silicon nitride bridge not properly released after anisotropic etching. Greyscale image obtained with an optical microscope (10× magnification).

3.4 DISCUSSION & CONCLUSION

*Almost the entire
fabrication process
was observed*

Summarizing, two types of chips were fabricated: two wafers with structures made out of silicon oxide and two wafers with structures made out of silicon nitride. The most important structures are sketched in fig. 2. Both types contain many structures with gold patches, e.g. at the tip of cantilevers. The fabricated structures made from silicon oxide and silicon nitride are in principle identical as the same masks have been used in both cases. Figure 2 shows the three most important device designs (cantilevers, paddles, bridges) that make out the majority of the wafers. One wafer of each type has been diced without releasing the structures. These chips are more robust for performing surface chemistry and analysis as they don't contain fragile, free standing structures. The others two wafers comprise fully prepared chips with released microcantilevers that can be analyzed, for instance, with a laser Doppler vibrometer (LDV).

4 | EXPERIMENTAL WORK

To functionalize the fabricated cantilevers in such a way that they gain biosensing properties, various steps have to be performed. This chapter explains how the chosen surface chemical functionalization strategy is applied, how the key experiments are executed and what techniques are used to perform these experiments. First, the sample preparation is described. Cantilever experiments are structured in three chronological rounds.

4.1 SAMPLE PREPARATION

All samples are cleaned by exposure to oxygen plasma (SPI Plasmaprep II) for 10 min, followed by immersion in pure ethanol for 20 minutes. The first step oxidizes any organic contaminants present on the surface to volatile products such as for instance water and carbon dioxide, whereas the second step reduces the gold oxide formed on the gold surface during the oxygen plasma treatment back to metallic gold [Ron et al., 1998]. In literature, the use of piranha solution is frequently reported for this cleaning step [Kosaka et al., 2013]. However, because of the reactivity and toxicity of piranha, this is avoided here. Besides, it is also reported that the electrochemical characteristics for the self-assembly of thiol-modified DNA layers hardly depend on the gold pretreatment [Li et al., 2014]. DNA molecules are purchased from *Eurofins* and prepared according to the supplier's manual. TE-buffer is used as the recommended solvent. Directly before all measurements, samples are rinsed with ethanol and dried in a flow of nitrogen.

Samples are cleaned with oxygen plasma and ethanol

4.2 ROUND 1

Two key functionalization steps are performed in experimental round 1.

1. Immobilization of Thiol-ssDNA
2. Hybridization with complementary DNA

A silicon nitride chip is immersed in a 1 μ M solution of thiolated single-stranded DNA in TE-buffer overnight. This gives the probes sufficient time to bind to the gold coated surface of the cantilevers. The DNA strands used for the experiments in this thesis are short 21-base-pair strands. The probes with a thiol linker at the 5' end have the base sequence: GCGTGCCAACGCGCTGCAT (5' \rightarrow 3') The cantilever chip is rinsed with ethanol and then immersed in the hybridization solution for 60 h at 50 °C. The complementary DNA is modified with a fluorescence tag (Cy5) and has the base sequence: ATGCGCAGCGCGTTGGCACGC Before and after each step, the resonance frequencies of all cantilevers is mea-

See fig. 10 for a visualization of the immobilization step

sured by laser Doppler vibrometry. This holds for all three rounds of cantilever experiments.

4.3 ROUND 2

The goal of round 2 is the verification of reproducibility of the results found in round 1. Therefore, the following two functionalization steps have been performed.

1. Immobilization of Thiol-ssDNA
2. Hybridization with complementary DNA and non-complementary control

Non-complementary control

The procedure is analogue to the first experimental round apart from the fact that two chips are functionalized in parallel. While the first step is exactly identical for both chips, in the second step one chip is immersed in complementary DNA solution and the other one in non-complementary DNA solution. The non-complementary DNA target has the same base sequence as the thiolated probe and can therefore not hybridize with it. The hypothesis is that there is a difference in resonance frequency shift between the two chips. While the resonance frequency of the chip immersed in complementary DNA solution should change due to hybridization, the resonance frequency of the control chip should ideally not shift at all. The elevated temperature is known to thermodynamically lower the non-specific adsorption and thereby the temperature facilitates the discrimination between complementary and non-complementary DNA. The chips are immersed in the hybridization solution for 85 h.

4.4 ROUND 3

The goal of round 3 is the reduction of non-specific adsorption to further increase the difference in cantilever response between hybridization with complementary and non-complementary DNA. Therefore, the following three steps are performed in experimental round 3.

Backfilling with PEG-Silane to decrease non-specific adsorption

1. Immobilization of Thiol-ssDNA
2. Backfilling with Silane-PEG
3. Hybridization with complementary DNA and non-complementary control

The first and third step are performed the same way as explained in round 1 and 2. The backfilling step has not been performed before. A visualization of the functionalization strategy is given in figs. 10 to 12.

PEG-Silane has to be handled in a dry, oxygen-free environment. Therefore, 10 mg PEG-Silane is weighted on a balance in a nitrogen glove box and given in a small flask, sealed airtight with a septum and carried to a fume hood. 10 mL of a 95 % ethanol, 5 % H₂O mixture is degassed by bubbling nitrogen for 10 min and then injected with a syringe through the septum into the flask containing PEG-Silane. Dissolution is enhanced by putting the mixture in an ultrasonic bath for 2 min. 5 mL of this mixture are poured into a beaker containing the silicon nitride chip and another 5 mL are used to backfill a second chip for the control experiment. This step is performed under a funnel through which

nitrogen is blown. The chips are immersed in the PEG-Silane solution for 1 hour. Hybridization time is again 85 h.

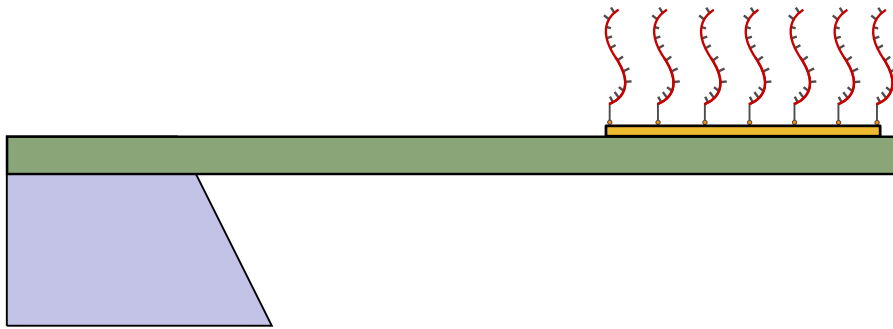


Figure 10: Schematic drawing of thiol ssDNA probe (red) immobilization step. Dimensions not drawn to scale.

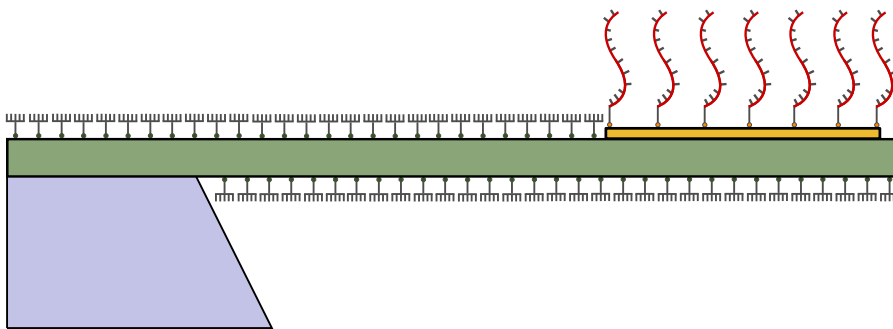


Figure 11: Schematic drawing of backfilling step with PEG-Silane after thiol ssDNA probe immobilization step. Dimensions not drawn to scale.

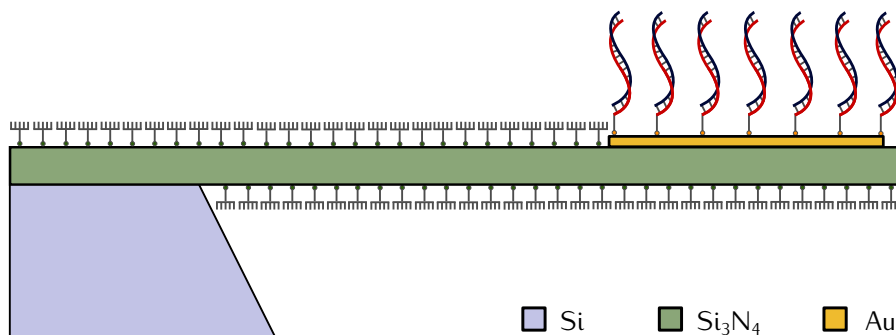


Figure 12: Schematic drawing of hybridization step with complementary DNA target (blue). Dimensions not drawn to scale.

4.5 LASER DOPPLER VIBROMETRY

A laser Doppler vibrometer (LDV) is a scientific instrument that enables optical vibration measurements without physical contact to the sample. Based on the Doppler effect, the vibrometer senses the frequency shift of laser light scattered back from a moving surface. The system uses a Fast Fourier Transform (FFT) to determine the amplitude of vibration over a selected frequency spectrum. For

Most measurements in this thesis are done with the LDV

the frequencies of interest, the frequency resolution is about 1.5 Hz and the amplitude noise level is as low as a few pm (Polytec OFV-552). This impressive sensitivity is needed in fact as the Brownian motion vibration amplitude of the cantilevers due to thermal actuation at room temperature is experimentally found to be only at the order of some 10 pm, thus only 1 order of magnitude above the noise level. For the cantilevers without a piezoelectric actuation layer as used in this thesis, electric read-out with an impedance analyzer is not possible and therefore an optical read-out has to be used. The LDV is a fast, easy, and highly precise tool for this task.

4.6 SCANNING ELECTRON MICROSCOPY AND ENERGY DISPERSIVE X-RAY SPECTROSCOPY

Scanning electron microscopy uses a finely collimated beam of electrons focused onto a small probe that scans along the surface of a sample. Interactions between the incident beam and the material result in the emission of electrons and photons. These emitted particles are analyzed by suitable detectors and give information about the surface topology of the sample, which is reconstructed to an image with impressive nm resolution of the sample surface. Energy dispersive X-ray spectroscopy (EDS) is a useful technique for analyzing the chemical composition of the surface of a specimen with an information depth of about 1000 nm and is often included in a scanning electron microscope. In EDS, the atoms on the surface of a specimen are excited by an electron beam, emitting specific wavelengths of X-rays which are characteristic for the atomic structure of an element. An energy dispersive detector can analyze these X-rays and assigns the appropriate elements. SEM and EDS are usually performed in a high vacuum [Ebnesajjad, 2014]. The SEM (Zeiss Merlin HR FEG) was operated by Mark Smithers.

*Samples of round 1
and 2 are
characterized by
SEM-EDS*

4.7 X-RAY PHOTOELECTRON SPECTROSCOPY

X-ray photoelectron spectroscopy (XPS), also called electron spectroscopy for chemical analysis (ESCA), is an analytic technique to characterize surfaces with an information depth of about 10 nm and is able to detect all elements except hydrogen. A sample is irradiated by X-ray beams which provide the energy needed for inner shell electrons to escape from the sample surface. A detector measures the kinetic energies of these photoelectrons, which is equal to the electrons' binding energies. This in turn allows the identification of the elements on the surface [Ebnesajjad, 2014]. Survey scans are made to see the gross overall atomic content of the surface layer. Element spectra scans are made with a better energy resolution and lower noise. From these scans, the atomic concentrations of the elements can be calculated. XPS is used in this project to characterize the gold coated cantilever tip with the goal to detect sulfur and phosphorus as markers for thiol-groups and DNA, respectively. The XPS (Quantera SXM) was operated by Gerard Kip.

*Samples of round 2
are also analyzed by
XPS*

4.8 FLUORESCENCE MICROSCOPY

In Fluorescence microscopy, samples are illuminated with light of a specific wavelength that is absorbed by the fluorophores, molecules with which the species of interest must be labeled in advance. These fluorophores emit wavelength of longer wavelength, thus a different color than the adsorbed light, which can be separated from the illumination light in a spectral emission filter. The filter and the dichronic have to be chosen to match with the spectral excitation and emission characteristics of the fluorophore used to label the specimen. The fluorescence microscope used is an Olympus IX71.

All functionalized cantilevers were examined by fluorescence microscopy

4.9 SURFACE PLASMON RESONANCE

A surface plasmon resonance sensor (SPR) is a label-free and surface sensitive spectroscopic system which optically measures changes in the local index of refraction on a metallic surface, typically a thin gold layer on a glass substrate. Thereby, it is sensitive to changes in the adsorption layer. SPR is an established technique in the field of biomolecular interaction analysis including dynamic analysis of DNA hybridization [Chung et al., 2012].

SPR is used in this project as a check whether the chosen chemical functionalization sequence works on gold surfaces independently from any cantilever mechanics. A standard, commercial gold sample, 50 nm Au on glass, is cleaned in piranha solution (3:1 mixture of sulphuric acid H_2SO_4 and hydrogen peroxide H_2O_2) for 1 minute, subsequently rinsed with copious amounts of demineralized water and afterwards immersed in ethanol for 5 minutes. The sample is immersed in the solution of thiol-terminated single stranded DNA overnight for probe immobilization through thiol-gold binding. Backfilling is performed by 1 h immersion in MUHEG, a thiol-terminated oligoethylene glycol (see section 2.7). First, non-complementary DNA solution is flushed through the system and over the gold chip with the SAM of thiol-ssDNA. Then the system is washed with TE buffer before the flow of complementary DNA solution is started. Eventually, the lines are washed with TE buffer again. The SPR (Res-tec RT 2005) was operated by Roberto Ricciardi.

4.10 DISCUSSION & CONCLUSION

Summarizing, three rounds of cantilever experiments have been performed, in which silicon nitride cantilevers were subsequently functionalized by thiol-ssDNA probe immobilization, backfilled with PEG-Silane as anti-fouling agent, and hybridized with complementary DNA and non-complementary control. For characterization and analysis, laser Doppler vibrometry, scanning electron microscopy and energy dispersive X-ray spectroscopy, X-ray photoelectron spectroscopy, fluorescence microscopy, and surface plasmon resonance are used.

5 | RESULTS

This chapter presents the results of three rounds of cantilever functionalization experiments and a reference experiment by surface plasmon resonance (SPR). Furthermore, silicon oxide devices are characterized and the time effect of immersion in TE-buffer on the resonance frequency of silicon nitride cantilevers is shown.

5.1 ROUND 1

In the first experimental round, one Si_3N_4 chip was used. The resonance frequency of five cantilevers, of which three possess a gold patch at the tip, was measured before and after thiol-ssDNA probe immobilization. Figure 13 shows the relative shift in resonance frequency $\frac{\Delta f}{f}$ in percent. Therefore, the difference in resonance frequency has been divided by the initial frequency of the clean cantilever before immobilization. The error bars are calculated by taking a possible error of 5 Hz into account for each LDV measurement. This value is chosen empirically as the LDV data processing involves a semi-manual peak fitting step. 5 Hz is more than three times larger than the frequency resolution of the LDV measurement (1.5 Hz) in the region of interest (< 20 kHz). The same cantilevers have been used in the second step, the hybridization with complementary DNA. Surprisingly, the response of cantilevers without gold is larger than the response of cantilevers with a gold patch at the tip (see fig. 14). The resonance frequency shift is stable even after the chip lay in a sample box in air for three days (blue column in fig. 14). Additional rinsing with ethanol does not change the resonance frequency significantly (green column in fig. 14).

$$\frac{\Delta f}{f} = \frac{f_{\text{after}} - f_{\text{before}}}{f_{\text{before}}}$$

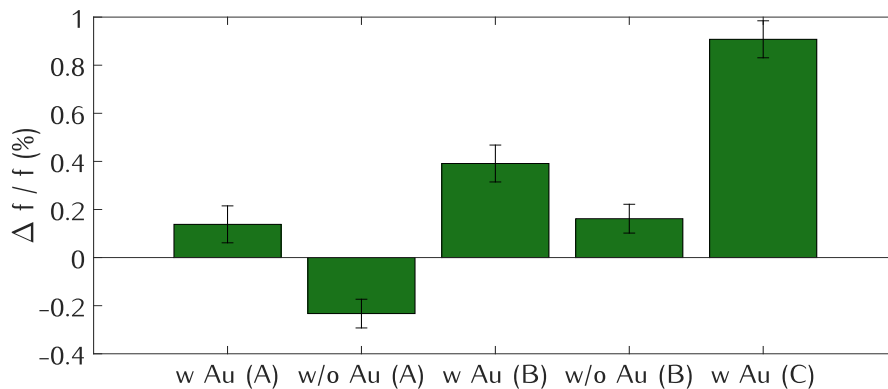


Figure 13: Relative resonance frequency shift of cantilevers with and without gold due to probe immobilization of thiol-ssDNA.

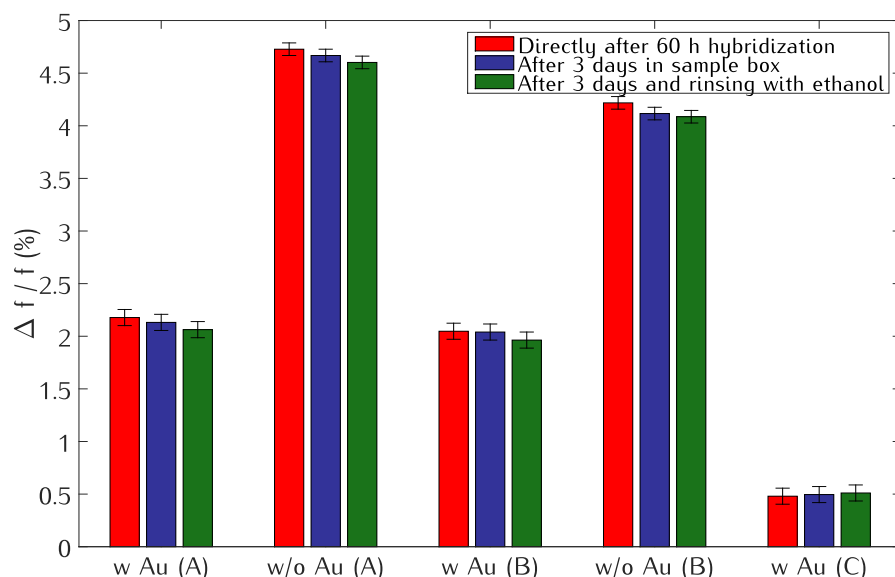


Figure 14: Relative resonance frequency shift due to hybridization with complementary DNA. The frequency shift is given with respect to the resonance frequency after probe immobilization. Measurements are taken directly after hybridization step (red), 3 days later (blue), and after rinsing with ethanol (green).

5.2 ROUND 2

In the second experimental round, two Si_3N_4 chips were functionalized simultaneously. After common thiol-ssDNA probe immobilization, one chip was immersed in a solution of complementary DNA and the other was immersed in a solution of non-complementary DNA. Other than that, the experimental conditions were identical. The results are presented in fig. 15, where the relative frequency shift due to the hybridization step is shown. There is a clear difference in resonance frequency shift between cantilevers on the chip that was immersed in complementary DNA solution for hybridization and those cantilevers on the other chip that was in non-complementary DNA solution as control experiment. This means the applied cantilever functionalization route is specific to the complementary DNA strand and a future sensor using these cantilevers can distinguish between complementary and non-complementary DNA. This is a very important result in the development of a sequence specific DNA sensor. Agreeing with the results of the first experimental round, the response of cantilevers without gold patch is much larger than the response of cantilevers that actually have a gold patch.

Frequency shift is larger for complementary DNA as compared to non-complementary DNA

XPS measurements were performed on both chips of round 2. A comparison of two representative spectra is shown in fig. 16. Six measurement points were chosen, four on gold coated cantilever tips and two on cantilevers without gold for control. It was intended to also scan phosphorus peaks, which would be characteristic for the presence of DNA on the cantilevers in our experiments, but unfortunately, the phosphorus $2p$ peak overlaps with a shake-up of the silicon $2p$ peak and the two cannot be distinguished in XPS measurements performed. Therefore, the sulfur $2p$ peak is, in fact, the only remaining marker for DNA in the XPS analysis. The analysis reveals that there is sulfur on the gold covered cantilever tips and no sulfur on the uncoated silicon nitride control

Sulfur is characteristic here for thiol-terminated ssDNA and only detected on gold coated cantilever areas

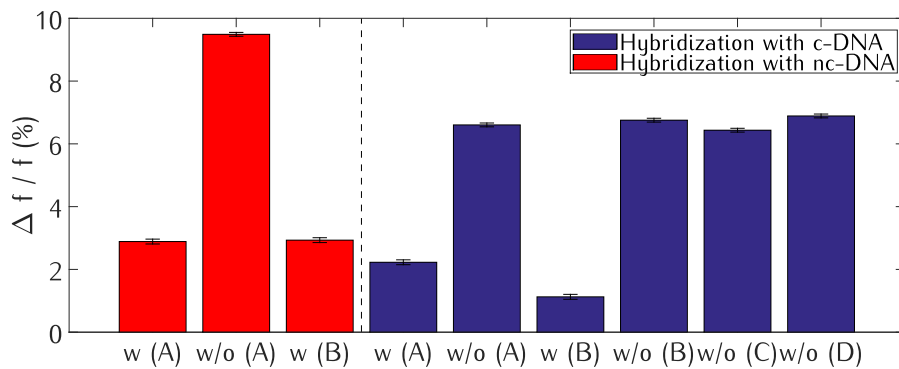


Figure 15: Relative resonance frequency shift due to DNA hybridization with respect to the resonance frequency after probe immobilization. Complementary on the left (red), non-complementary control on the right (blue).

cantilevers. The other four XPS spectra are given in appendix A.8 including a table of element concentrations. In fig. 17, the fluorescence intensity of two cantilevers that were used in round 2 is compared. The left cantilever was immersed in complementary DNA solution for hybridization and shines brightly on the uncoated Si_3N_4 areas. The cantilever shown on the right, which was immersed in non-complementary DNA solution, looks pale and shows only very pale fluorescence intensity. The gold areas on both cantilever appear completely black and no fluorescence intensity can be recorded there even with an increased camera exposure time.

Cantilevers that were immersed in complementary DNA look much brighter in fluorescence microscopy

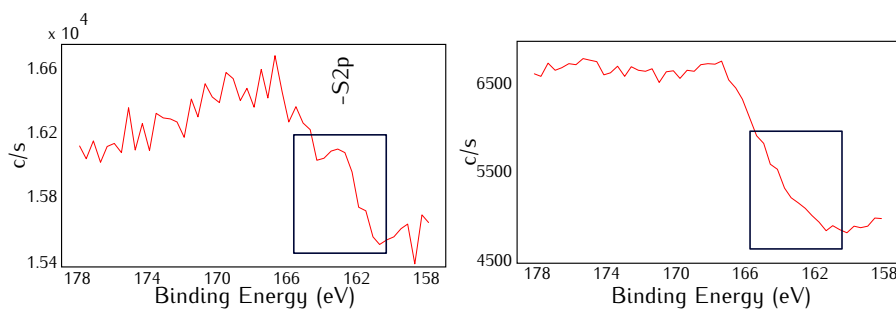


Figure 16: Comparison of sulfur peaks in XPS spectra. The left spectrum is taken on a gold patch and shows a shallow peak in the region of interest, the right spectrum, taken on a cantilever without gold, does not.

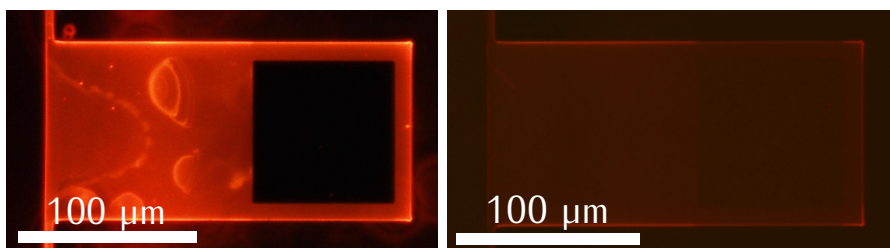


Figure 17: Comparison of fluorescence intensity. The left cantilever was immersed in complementary DNA solution, the right one in non-complementary DNA solution. Camera exposure time 4.00 s (l.) and 11.47 s (r.).

5.3 ROUND 3

Different from the first two experimental rounds, in round 3, backfilling with PEG-Silane is used to reduce non-specific adsorption. Figure 18 shows the relative frequency shift due to the backfilling step. Prior to this step, thiolated ssDNA was immobilized on the gold coated cantilever surface. Sign and magnitude of the frequency shift vary largely. The outlier, cantilever F (rightmost column in fig. 18 and 19), is the same cantilever that already appears as outlier in the first experimental round (see rightmost column in fig. 13 and 14). The reason why this particular cantilever shows an aberrant response is analyzed in detail and discussed in section 6.1. The fluorescence microscopy images closely resemble the ones recorded in round 2 (see fig. 17) and are provided in appendix A.7.

Figure 19 shows a large difference in sensor response between hybridization with complementary DNA and non-specific adsorption

Figure 19 shows the most important finding of this thesis. While the frequency shift of the cantilevers that were immersed in complementary DNA solution for hybridization (red) is in agreement with the first two experimental rounds, the frequency shift of the control cantilevers that were in non-complementary DNA solution (blue) is completely different. Even the sign of the frequency shift is switched. From the data presented in fig. 19, it is easy to distinguish the hybridization of complementary DNA from non-specific adsorption in the control experiment.

5.4 SURFACE PLASMON RESONANCE

The same chemicals as in the first round of cantilever experiments have been used for an SPR experiment. The following steps have been performed on a sample that was prepared by overnight DNA immobilization and backfilling with MUHEG as explained in section 4.9. After 12 min, flushing non-complementary DNA with a concentration of 1 μM in TE buffer was started; after 48 min, washing with TE-buffer was initiated. At 2 h 15 min, complementary DNA 1 μmol in TE buffer was flushed and eventually, at 3 h 5 min, the sample and lines were washed with TE-buffer again.

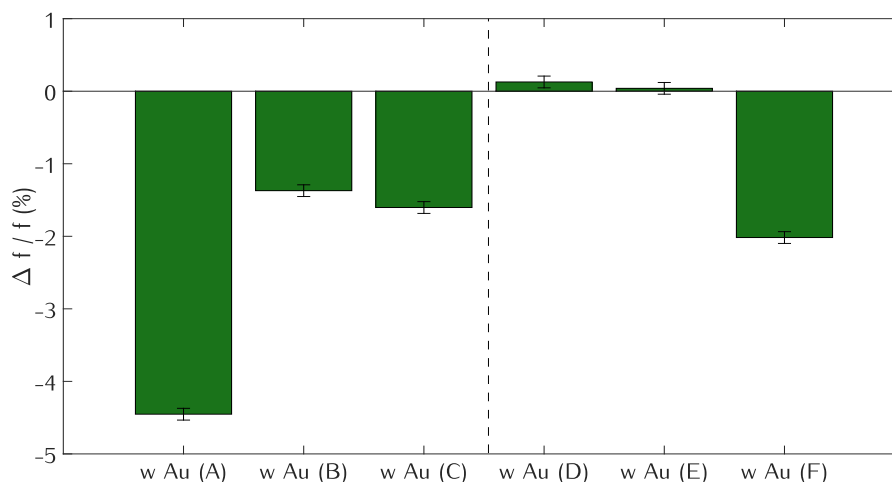


Figure 18: Relative resonance frequency shift due backfilling with PEG-Silane.

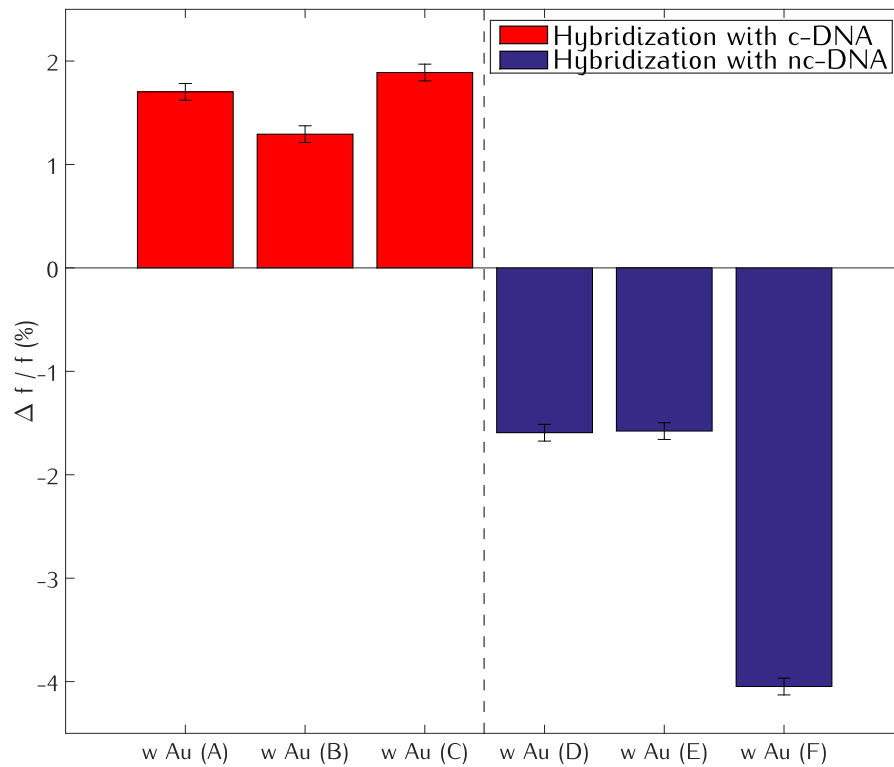


Figure 19: Relative resonance frequency shift due to DNA hybridization with respect to the resonance frequency after backfilling. Hybridization with complementary DNA on the left (red), non-complementary control on the right (blue).

The outcome of this experiment is shown in fig. 20 where the noisy measurement data is accompanied by a guide to the eye, a line that is computed by applying a least squares smoothing function over 50 neighboring data points per position. The measured change in angle $\Delta\theta$ is only in the range of 1×10^{-3} deg during the entire experiment and there is no distinct response to any of the components that were flushed during the experiment.

The SPR does not show any response to the DNA solution

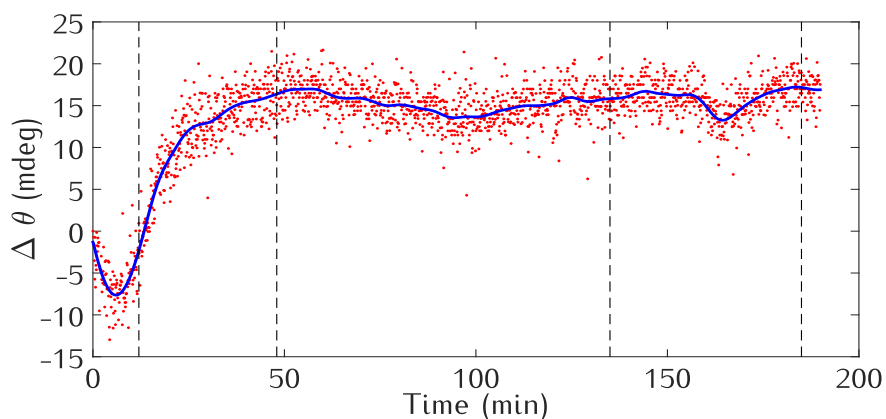


Figure 20: SPR measurement data (red) and smoothed line as guide to the eye (blue). Dashed vertical lines indicate when the following steps were performed: Starting flow of non-comp. DNA solution, washing with TE buffer, flowing comp. DNA solution, washing with TE buffer again.

5.5 SILICON OXIDE DEVICES

The fabricated silicon oxide devices cannot be analyzed by LDV due to strong out-of-plane bending

By visual inspection under an optical microscope the gold tip of all silicon oxide cantilevers looks dark. Out of plane bending can explain this. This hypothesis was verified by scanning electron microscopy. Figure 22 shows a micrograph of a silicon oxide chip with three paddle-type cantilever in a microfluidic channel. The bottom paddle is shown in a close-up with a higher magnification in fig. 23. All cantilevers, but particularly those with a gold coated tip, are bent out of plane. Laser Doppler vibrometry is not possible with these devices, as the curvature of the devices reflects the laser beam under an angle which is too large for the detector. Multiple attempts were conducted and also slightly tilting the sample did not help.

5.6 TIME EFFECT OF THE TE - BUFFER

TE-buffer causes increase in resonance frequency over time

Figure 21 shows how the resonance frequency of silicon nitride cantilevers changes as a function of time when they are immersed in pure, DNA-free TE-buffer at room temperature. Measurements are taken on three identical cantilevers with a gold patch at the tip. These cantilevers are on the same chip. Prior to each measurement, the chip is rinsed with ethanol and dried under a flow of nitrogen. After ~ 30 h, saturation sets in and the relative frequency shift remains at $\sim 1\%$. Cleaning with 10 min oxygen plasma and subsequent immersion in ethanol for 20 min lowers the resonance frequency by 3%. All shifts are given relative to the initial, clean state.

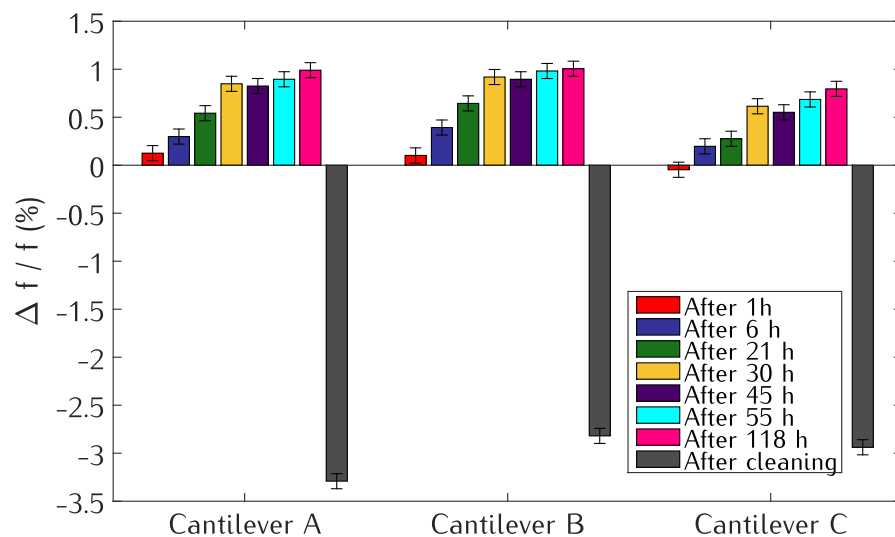


Figure 21: Resonance frequency shift of 3 Si_3N_4 cantilevers with Au at tip after 1, 6, 21, 27, 60, 118 h in TE-buffer and finally cleaned again.

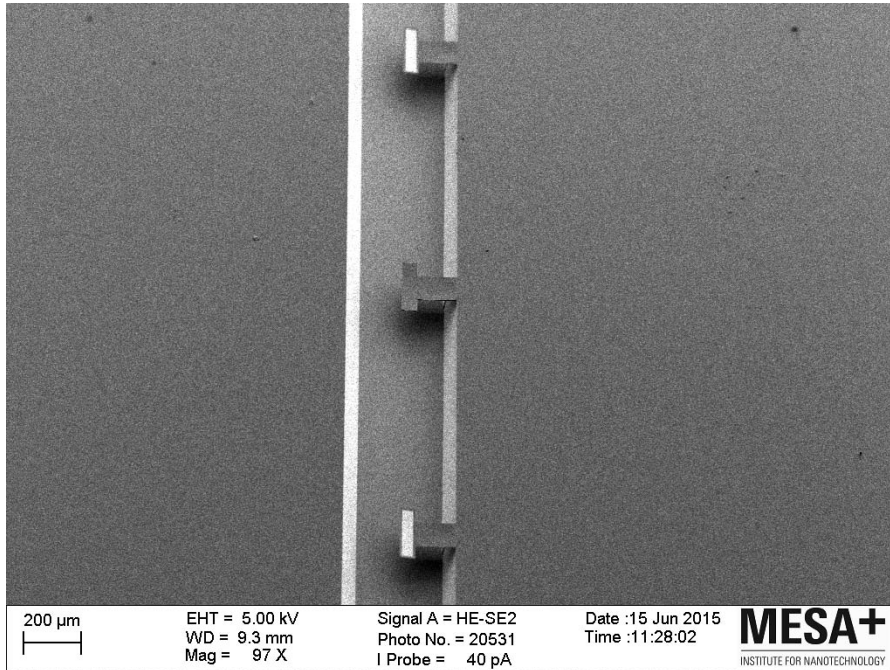


Figure 22: SEM micrograph of a silicon oxide chip with three paddle-type cantilevers; the outer ones possess a gold patch at the tip, the center one does not. The slanted walls of the microfluidic channel created by anisotropic wet etching appear lighter than the surrounding flat surface

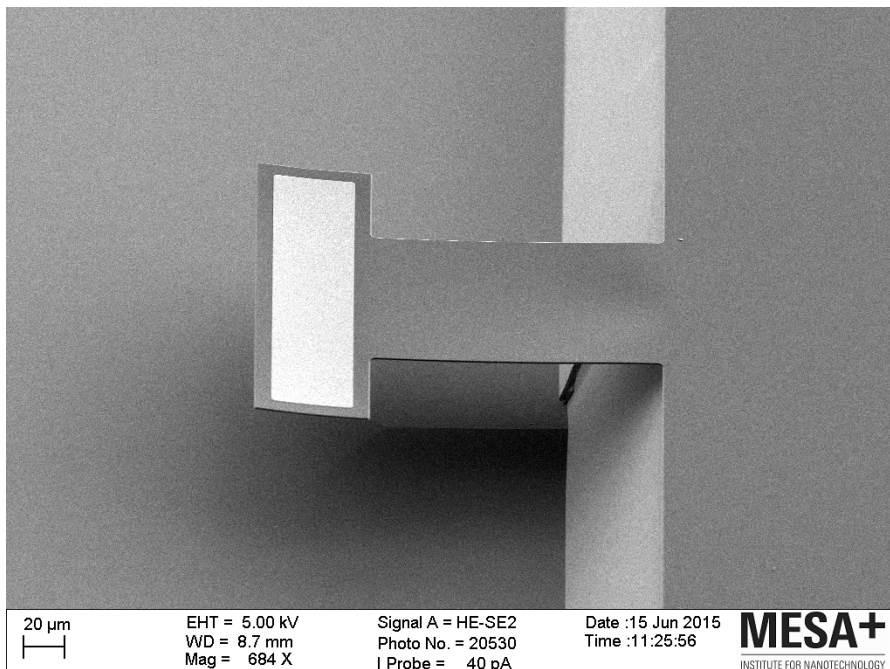


Figure 23: SEM micrograph of gold coated silicon oxide paddle-type cantilever bent out of plane. Close-up of the bottom structure shown in fig. 22

6 | DISCUSSION & RECOMMENDATIONS

Multiple experimental results have been presented on the previous pages. The purpose of this chapter is to discuss them in depth by interpreting and comparing them, connecting data obtained by various techniques to get a coherent picture, and reflecting upon the initial goals of this thesis. In addition, suggestions for further research are given.

6.1 EXPERIMENTAL ROUND 1

In the first experimental round, a silicon nitride chip is functionalized by tethering thiolated single stranded DNA molecules to the gold coated cantilever surface. This changes the mass, surface stress, and stiffness of the cantilevers and results in a resonance frequency shift. Figure 13 shows how the latter differs in sign and magnitude from cantilever to cantilever. The second and far more important step, the hybridization step, where the actual biorecognition event takes place, gives a more consistent result (see fig. 14).

Looking at fig. 13 and 14, there is one real outlier, namely the rightmost column. This cantilever is examined additionally by SEM-EDS. It is found to be aluminum debris that disturbs the properties of this particular cantilever. This aluminum probably originates from a piece of aluminum foil that was used to cover a beaker of DNA solution. Optical and fluorescence microscopy images, SEM micrographs and EDS spectra of this cantilever are provided in appendix A.5.

The SPR results presented in fig. 20 does not show any response to the components that were flushed subsequently. The same molecules as in round 1 were used for the SPR measurement. A possible explanation for this is that the DNA hybridization of a 21 base pair DNA strand is below the sensitivity limit of the SPR equipment used. This hypothesis can be tested in future experiments with longer and thus heavier DNA strands.

The SPR experiment performed is inconclusive and cannot be used as a reference

6.2 EXPERIMENTAL ROUND 2

Aim of the second experimental round is the verification of the results obtained in the first round and adding a non-complementary control. The measured frequency shifts exhibit the same trends as in round 1. The magnitude of the relative frequency shift in round 2 is about 40% larger as compared to round 1. This coincides with a roughly 40% longer hybridization time of 85 h in round 2 compared to 60 h in round 1. While DNA hybridization naturally has to saturate given only a finite number of immobilized ssDNA probes on the gold tip of the cantilevers, this finding indicates that something else is happening. Saturation

is reported to set in after ~ 12 h, a time span much shorter than the minimal 60 h used here [Hagan and Chakraborty, 2004; Henry et al., 1999].

In order to exclude effects of the TE-buffer solution, a clean Si_3N_4 chip is immersed in pure TE-buffer for a long time and its resonance frequency is measured repeatedly. The results shown in fig. 21 reveal that it is not the buffer solution that causes the large magnitude of sensor response.

The goal of fluorescence microscopy in the context of this project is the verification of the areal density of (hybridized) DNA. However, under the fluorescence microscope, the gold coated cantilever tip areas look totally black. This agrees with previous results of the *Inorganic Materials Science* group and can be explained by quenching of fluorescence on gold. X-ray photoelectron spectroscopy (XPS) is therefore used to characterize the elemental composition at the bare and gold coated cantilever surfaces.

The XPS data shows the presence of sulfur on gold areas (see fig. 16) indicating that the first step of the chemical cantilever functionalization, the immobilization of thiolated single-stranded DNA probes on gold, is indeed successful. Despite the fact that the signal is rather weak, the finding of sulfur is a proof for the presence of thiol-ssDNA. However, the XPS cannot fully replace fluorescence microscopy. The latter, in principle, allows a differentiation between complementary DNA hybridization and non-specific adsorption when different fluorophores are used. XPS, which analyses the atomic concentrations at a surface, cannot do this as all types of DNA contain phosphorus and all thiolated DNA probes contain sulfur irrespective whether they are complementary or not.

*Noticeable difference
in cantilever
response between
hybridization with
complementary DNA
and non-specific
adsorption*

From the fluorescence microscopy images, no information can be deduced about the quenching gold areas. There is, however, a strong difference in fluorescence intensity on the silicon nitride areas of the cantilevers between the chip that was immersed in complementary DNA solution and the one that was immersed in non-complementary DNA solution (see fig. 33). This qualitative finding suggests that there might still be traces of thiolated ssDNA on the silicon nitride areas, too small to be detected by the XPS, which hybridized with complementary DNA targets. The fluorescence intensity of the cantilevers immersed in non-complementary solution is much weaker indicating less non-specific adsorption compared to complementary hybridization. The measured resonance frequency shifts of the cantilevers confirm this hypothesis. The difference in relative frequency shift between the complementary DNA hybridization and non-specific adsorption is small but noticeable.

6.3 EXPERIMENTAL ROUND 3

*Anti-fouling agent
increased the
specificity of the
cantilever response*

In experimental round 3, the two step process of probe immobilization and target recognition by DNA hybridization is supplemented by an intermediary backfilling step. The goal of backfilling is a reduction of non-specific adsorption, which can lead to false-positive sensor response. Comparing fig. 15 and 19, this goal is clearly achieved. Due to backfilling with PEG-Silane, the difference in resonance frequency shift between hybridization with complementary DNA and non-specific adsorption is much larger as in experimental round 2, where no anti-fouling agent was used.

6.4 APPLICABILITY OF THE THEORETICAL MODEL

The measured response of cantilevers without a gold patch is stronger than the response of those cantilevers that actually have a gold patch. This counter-intuitive finding is consistent in all three experimental rounds and could be explained in the following way: Silicon nitride often contains space charges. These charges could electrostatically attract DNA, which is also charged [Ravan et al., 2014]. These electrostatic forces can also explain why the measured sensor response is orders of magnitude larger than predicted in the theory section. If namely electrostatic forces are dominant, it is not self-assembled monolayer adsorption which takes place, but instead a rather thick layer of DNA is attracted to the cantilever surface. This is in agreement with the fluorescence detected on the silicon nitride areas of the cantilevers. Yet, this leads to the conclusion that more effects than initially expected play an important role. Most likely, the DNA does not form self-assembled monolayers limited to the gold covered cantilever tips, but rather thick adlayer all around the entire cantilever. Even the most recent theoretical model for the adsorption of biomolecules on a cantilever surface by Ruz et al. [2014] cannot explain the large frequency shifts observed otherwise.

Summarizing, if it is indeed the case that electrostatic forces from space charges cause the attraction of thick DNA layers, it is questionable whether the silicon nitride chips fabricated for this thesis are reliable biosensors for DNA sensing applications. Cautious optimism is justified by the fact that there is a clear and consistent difference in cantilever response between chips that were immersed in complementary DNA solution and those that were immersed in non-complementary DNA solution (see fig. 15 and 19). From this it is possible to differentiate the hybridization of complementary DNA strands from non-specific adsorption, which is the goal of the proposed sensor device. However, the number of chips analyzed is very small. In total, only four silicon nitride chips were used. Kosaka et al. [2013] rightly argue that it needs large arrays of microcantilevers for a statistical approach to tackle reproducibility problems.

The stress effect might be underestimated by the model given in section 2.4.2. Most prominently, there must be very large stresses that cause the out-of-plane bending of the silicon oxide devices (see fig. 23). Furthermore, a cantilever with a low aspect ratio inherently has a surface stress gradient due to clamping effects [Tamayo et al., 2013]. Substituting the dimensions and properties of the cantilevers used into Tamayo's correction to Stoney's equation, a difference of 25% in surface stress along the cantilever beam is obtained. However, the frequency shift due to surface stress of the DNA adlayer is predicted to be at the order of a few ppm only. Even a variation of 25% does obviously not increase this value by orders of magnitude and therefore this surface stress effect of the adlayer is still expected to be negligible. This conclusion is in agreement with the results found by Ramos et al. [2009].

The vast amount of physical, mechanical, and chemical parameters that have an influence on the functioning of a cantilever sensor makes it so hard to develop an all-encompassing, precise model for the transduction process of a cantilever biosensor. At the moment, we do not fully understand all the involved processes yet. However, the experimental results presented in this thesis are very promising when looking back on the ultimate goal of the project: a sensor that can detect (hypermethylated) DNA sequence specific.

It is possible to distinguish hybridization of complementary DNA from non-specific adsorption by the different shifts of cantilever resonance frequency

6.5 RECOMMENDATIONS FOR FURTHER RESEARCH

Temperature and humidity effects on cantilever resonance frequency are recommended to be examined in future work

Future sensors have to tackle even more issues. In fact, the concentration of free DNA in urine is low. The DNA that is actually hypermethylated and can act as a biomarker for bladder cancer as described in the introduction, is again only a small fraction of the already low concentration of free DNA in urine.

Future work should examine the effect of temperature and humidity on a micro-cantilever sensor. Unpublished calculations by dr. Evert Houtman, a colleague researcher of the *IMS* group, predict a frequency shift of -31.2 ppm / K for a bare silicon cantilever. Besides, many material properties are known to change with temperature. Thermal mismatch between different materials in a multilayered cantilever can affect the resonance frequency [Shen et al., 2001]. Hydration induced tension forces in nucleic acid SAMs are reported to be strong enough to bend microcantilevers. Therein, a clear difference between monolayers that interact with either complementary DNA or non-complementary DNA targets can be observed with sensitivity in the femtomolar range [Mertens et al., 2008].

Figure 21, the time effect of TE-buffer, raises the question whether the cleaning procedure used (oxygen plasma and immersion in ethanol) alters the nature of the chip. Future work should test the effect of multiple repeated cleaning cycles on the resonance frequency of silicon nitride microcantilevers. Due to the limited time frame, it was not possible to repeat multiple cleaning and saturation cycles with TE-buffer.

To increase sensitivity of a cantilever sensor, the ratio of adsorbate mass to beam mass has to be decreased according to the mass and stiffness models. Therefore, smaller cantilevers are more sensitive. Apart from fabrication challenges, there is no obvious physical reason why smaller cantilevers would have disadvantages. Leading publications in this field report the use of substantially smaller cantilevers [Ramos et al., 2009; Ruz et al., 2014].

For the SPR measurement, the thiol-ssDNA probe layer on gold was backfilled with MUHEG, a thiol-terminated oligoethylene glycol (OEG). In cantilever experimental round 3, backfilling was performed with PEG-Silane. To further suppress non-specific adsorption, both strategies could be combined. Lokanathan et al. [2011] report that backfilling a PEG layer with OEG forms an underbrush structure enhancing the ability of the resulting layer to resist fouling. Ideally, MUHEG fills the voids between ssDNA on the gold and PEG-Silane forms an anti-fouling layer on the silicon oxide or nitride.

All doubly clamped beams, the bridges, were not released from the underside as can be easily seen under an optical microscope (see fig. 9). An attempt to characterize them with the LDV naturally has to fail. A longer anisotropic etch time is suggested for future wafers to deepen the microfluidic channel and thereby releasing the bridges eventually.

Unfortunately, none of the silicon oxide devices could be used for experiments with DNA simply because characterization with the laser Doppler vibrometer was not possible due to the strong out-of plane bending of the cantilevers. Therefore, the core experiments were, in fact, limited to cantilevers on four silicon nitride chips. Future silicon oxide cantilever devices must be fabricated differently such that there is less stress causing the undesired static out of plane bending. Otherwise the chips are not useful for this project.

7 | CONCLUSION

This thesis started with a comprehensive literature study in chapter 1 exploring the embedding of a nanomechanical cancer sensor. The theoretical framework was provided in chapter 2. In chapter 3, the fabrication of novel silicon nitride and oxide microcantilever devices was described. Chapter 4 introduced the techniques and methods used for the experimental work in this thesis. The results were shown in chapter 5 and discussed in chapter 6. The purpose of this chapter is to summarize the conclusions from the theoretical and practical work.

The cantilever resonance frequency shift is consistently found to be much larger than any of the theoretical models published in literature can explain. The large magnitude of the sensor response and the fluorescence intensity on silicon nitride areas lead to the conclusion that a layer of DNA, much thicker than a monolayer, is electrostatically attracted to the cantilevers. This thick layer causes an increase in stiffness that raises the cantilever resonance frequency. This explains why the response of silicon nitride cantilevers without a gold patch is consistently higher than the response of those without gold.

Silicon nitride electrostatically attracts a thick layer of DNA

Nevertheless, the results found and presented in this thesis allow cautious optimism. The hybridization of complementary DNA is successfully distinguished from non-specific adsorption. Without a dedicated anti-fouling strategy, however, the difference in sensor response is low, as experimental round 2 shows. Backfilling with PEG-Silane enormously improves the sensor performance. This is the core finding of experimental round 3. It is recommended that future work focuses on strategies to further enhance the blocking of non-specific adsorption and thereby improves the specificity of the proposed biosensor. The theoretical work suggests that sensitivity has to be increased by further downscaling of the cantilevers.

PEG-Silane anti-fouling layer greatly improves sensor performance

Due to quenching, fluorescence microscopy is found to be an unsuitable tool to verify the presence of DNA on gold coated cantilevers. XPS has shown to have intrinsic difficulties with the detection of sulfur and phosphorus in the presence of silicon.

Eventually, the DNA strands used in the functionalization experiments were short 21-base-pair strands, although the title of this thesis might readily suggest the use of hypermethylated DNA. The title is kept to embed the work of this thesis project in the bigger picture of the *Nanopill 2.0* project. The results presented in this thesis are small, but essential steps towards the final goal of a nanomechanical, cantilever-based DNA sensor for the detection of bladder cancer.

A | APPENDIX

This appendix supplies additional material to various sections of the thesis. It is structured as follows: In appendix A.1, the derivation of an analytical expression for the resonance frequency of a cantilever beam is given, followed by a correction term for cantilevers with a low aspect ratio in appendix A.2. In appendix A.3 and A.4, the mass and stiffness effects on the resonance frequency of the silicon nitride cantilevers used are computed. These four appendices complement the theory chapter (2). Appendix A.5 shows the detailed analysis of a cantilever that appeared as outlier in the experiments, which complements results from round 1 and 3. Appendix A.6 illustrates why the old generation of microcantilevers in the *Nanopill 2.0* project was unreliable and new devices had to be fabricated. Appendix A.7 shows additional fluorescence microscopy images taken in experimental round 3, and finally, appendix A.8 provides additional XPS data.

A.1 FLEXURAL VIBRATIONS OF A CANTILEVER

In the following, the partial differential equation describing free, transverse vibrations of a beam is derived via the energy approach and solved for cantilever boundary conditions.

Let the Lagrangian \mathcal{L} denote the difference between the kinetic energy T and the potential, strain energy U .

$$T = \frac{1}{2} \int_0^L \rho A \left(\frac{\partial v}{\partial t} \right)^2 dx \quad (8)$$

$$U = \frac{1}{2} \int_0^L EI \left(\frac{\partial^2 v}{\partial x^2} \right)^2 dx \quad (9)$$

$$\mathcal{L} = T - U = \int_0^L \left[\frac{\rho A}{2} \left(\frac{\partial v}{\partial t} \right)^2 - \frac{EI}{2} \left(\frac{\partial^2 v}{\partial x^2} \right)^2 \right] dx \quad (10)$$

v = v(x, t) is the deflection function of the beam

where E is the Young's modulus, ρ the material density, h the beam thickness, L the beam length, and $A = bh$ the cross-sectional area of the beam.

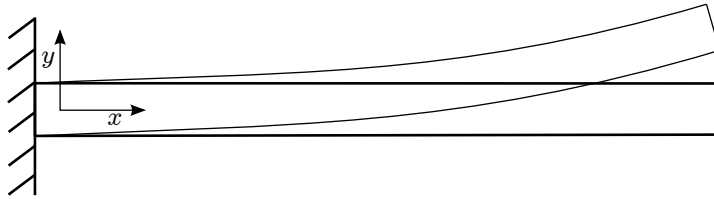


Figure 24: Cantilever beam with fixed end on the left and free end on the right

Applying the Euler-Lagrange principle yields the following differential equation for an Euler Bernoulli beam.

$$\rho A \frac{\partial^2 v}{\partial t^2} + EI \frac{\partial^4 v}{\partial x^4} = 0 \quad (11)$$

Boundary conditions: At the clamped end ($x = 0$), displacement and rotation are zero, whereas at the free end ($x = L$), shear force and internal bending moment are zero.

The boundary conditions must hold for all times t

$$v(0) = 0, \quad \frac{\partial v(0)}{\partial x} = 0, \quad \frac{\partial^2 v(L)}{\partial x^2} = 0, \quad \frac{\partial^3 v(L)}{\partial x^3} = 0 \quad (12)$$

Using separation of variables to mathematically split the function $v(x, t)$ that depends on space and time into a function $Y(x)$ that is only space-dependent and a function $T(t)$ that is only time dependent

$$v(x, t) = Y(x)T(t) \quad (13)$$

when substituted in equation (11) yields

$$Y\ddot{T} + c^2 Y''''T = 0 \quad (14)$$

$$c^2 = \frac{EI}{\rho A}$$

$$c^2 \frac{Y''''}{Y} = -\frac{\ddot{T}}{T} = \omega^2 \quad (15)$$

Superscript prime and dot denote a spacial and temporal derivative, respectively. Thus a set of two ordinary differential equations that have to be solved simultaneously is found

$$Y''''(x) - \frac{\omega^2}{c^2} Y = 0 \quad (16)$$

$$\ddot{T}(t) + \omega^2 T = 0$$

$$\lambda^4 = \frac{\omega^2}{c^2}$$

with general solution

$$Y(x) = c_1 \cosh(\lambda x) + c_2 \sinh(\lambda x) + c_3 \cos(\lambda x) + c_4 \sin(\lambda x) \quad (17)$$

$$T(t) = c_5 \cos(\omega t) + c_6 \sin(\omega t)$$

The boundary conditions of the clamped end (equation (12)) imply that

$$c_1 = -c_3, \quad c_2 = -c_4 \quad (18)$$

and the boundary conditions for the free end yield

$$\cosh(\lambda L) \cos(\lambda L) = -1 \quad (19)$$

which is, for instance, true for

$$\beta_1 = 1.87510, \quad \beta_2 = 4.69409, \quad \beta_3 = 7.85476, \quad \beta_4 = 10.9955, \dots \quad (20)$$

where $\beta_n = \lambda_n L$ denotes an eigenvalue. The first four numerical eigenvalues are given here.

This equation has infinitely many solutions which means there exist infinitely many modes for a freely vibrating cantilever.

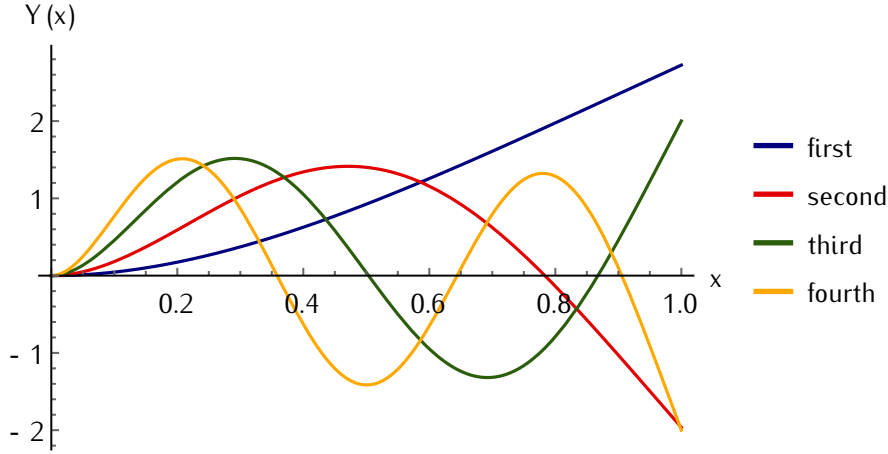


Figure 25: Cantilever deflection shapes $Y(x)$ for the first four transverse modes of a beam with normalized length, amplitude in arb. unit

Figure 25 shows the shape of the first four deflection functions for a cantilever beam with a length normalized to unity.

Using the the definition for λ we find for the resonance frequency

$$\omega_n = c\lambda_n^2 \quad (21)$$

and consequently

$$\omega_n = \beta_n^2 \sqrt{\frac{EI}{\rho AL^4}} = \beta_n^2 \sqrt{\frac{Eh^2}{12\rho L^4}} \quad (22)$$

$$f_n = \frac{\beta_n^2}{2\pi\sqrt{12}} \sqrt{\frac{E}{\rho}} \frac{h}{L^2} \quad (23)$$

which is equal to the result given by Tamayo et al. [2013]. $I = \frac{bh^3}{12}$ denotes the second moment of area and $A = bh$ the cross-sectional area of the cantilever beam.

A.2 LOW ASPECT RATIO OF THE CANTILEVER

In Looker and Sader's model, the angular resonant frequency of the Euler-Bernoulli model is multiplied with a correction term that depends on the width and length of the cantilever as well as on the Poisson's ratio of the cantilever material [Looker and Sader, 2008].

$$\omega_f = \omega_f^\infty \sqrt{\frac{1 + \mathcal{Z}(v)(b/L)}{1 + (1 - \nu^2)\mathcal{Z}(v)(b/L)}} \quad (24)$$

$$\mathcal{Z}(v) = \frac{4 \left(\sqrt{5}(1 - \nu) + \sqrt{1 - \nu^2} \right)}{\sqrt{3}\sqrt{1 - \nu^2} \left(5 - 5\nu - \sqrt{10}\sqrt{2 - 5\nu + 3\nu^2} + \sqrt{5 - 5\nu + \sqrt{10}\sqrt{2 - 5\nu + 3\nu^2}} \right)}$$

where ω_f^∞ is the angular resonant frequency as derived in equation (22) and ν denotes the Poisson's ratio.

The following values have been used in the computation

$$\begin{aligned} L &= 200 \mu\text{m}, \quad b = 100 \mu\text{m}, \quad h = 0.519 \mu\text{m}, \\ \nu &= 0.17, \quad E = 210 \text{ GPa}, \quad \rho = 3100 \text{ kg m}^{-3} \end{aligned} \quad (25)$$

Consequently, one obtains

$$\begin{aligned} f_{\text{LS}} &= 17\,140 \text{ Hz} \\ f_{\text{EB}} &= 16\,921 \text{ Hz} \end{aligned} \quad (26)$$

where subscript LS represents the model of Looker and Sader, and EB denotes the Euler-Bernoulli model. The difference between the two values is less than 2%, which largely explains the difference between the FEM model and the 1-dimensional Euler-Bernoulli model.

A.3 MASS EFFECT

The parameters given in table 4 are substituted in equation (2) to calculate the mass effect on the relative resonance frequency shift of a cantilever upon molecular adsorption. Here the calculation is summarized.

Total mass of the bare cantilever: 4.616×10^{-11} kg,

Au area: 6.400×10^9 nm²,

DNA monolayer density: 0.1 molecules /nm²,

Weight of one attached molecule (21-bp DNA + spacer + thiol): 7000 Da,

Total mass of adsorbed DNA monolayer: 4.480×10^{-12} kg,

Relative change in mass $\frac{\Delta m}{m} = 9.705 \times 10^{-5}$,

Relative resonance frequency shift: $\frac{\Delta f}{f} = -0.00485\%$,

Resonance frequency: 13045 Hz,

Absolute resonance frequency shift: $\Delta f = -0.633$ Hz.

A.4 STIFFNESS EFFECT

The evaluation of the equation for the stiffness effect (equation (4)) is challenging because of the fact that E_a , the Young's modulus of the adsorbate layer, ρ_a , its density, and h_a , its thickness, are unknown a priori. Even the properties of the

Table 4: Dimensions and properties of the silicon nitride cantilever needed for the calculation of the resonance frequency shift due to the mass effect of adsorbing molecules

Layer	L (μm)	b (μm)	h (μm)	ρ (kg m^{-3})	m (kg)
Si ₃ N ₄	200	100	0.519	3100	3.218×10^{-11}
Au	80	80	0.115	19000	1.398×10^{-11}

thin microbeams (subscript b) can differ from bulk values for silicon nitride. The following values are estimations and used in the computation.

$$\begin{aligned} E_a &= 1 \text{ GPa}, \quad \rho_a = 1700 \text{ kg m}^{-3}, \quad h_a = 10 \text{ nm} \\ E_b &= 1 \text{ GPa}, \quad \rho_b = 3100 \text{ kg m}^{-3}, \quad h_b = 519 \text{ nm} \end{aligned} \quad (27)$$

Relative resonance frequency change $\frac{\Delta f}{f} = -0.510\%$

A.5 ALUMINUM DEBRIS

From the fluorescence microscopy images it is deduced that fluorescence is quenched on the gold areas of the cantilevers. One outlier is found that - unlike all other cantilevers - shows a high fluorescence intensity on parts of the gold coated area (fig. 26). This cantilever is also an outlier in experimental round 3 (called w Au (F) in fig. 15). This cantilever is additionally analyzed by energy dispersive X-ray spectroscopy in a scanning electron microscope (SEM-EDS). Figure 27 shows an image taken with an optical microscope, fig. 28 a SEM micrograph. Figures 29 and 30 show EDS spectra of the debris. Au, Si, O, and C are elements expected to be found. Ti is used as adhesion layer between Si_3N_4 and Au. As the penetration depth of EDS is around $1 \mu\text{m}$, it is no surprise that a low percentage of Ti is recorded. The peak of P is very weak and not reliable. However, in this context, phosphorus is a marker for DNA. As the fluorescence image clearly shows there is definitely DNA on the debris. The debris itself is predominantly Al. A logical explanation for the origin of Al comes from the fact that the beaker of complementary DNA solution, where this chip was immersed in for the hybridization step, was covered with aluminum foil for some hours. Aluminum foil is not used anymore for covering beakers in experimental rounds 2 and 3.

The aluminum foil covering the beaker of complementary DNA solution caused Al debris on one of the cantilevers

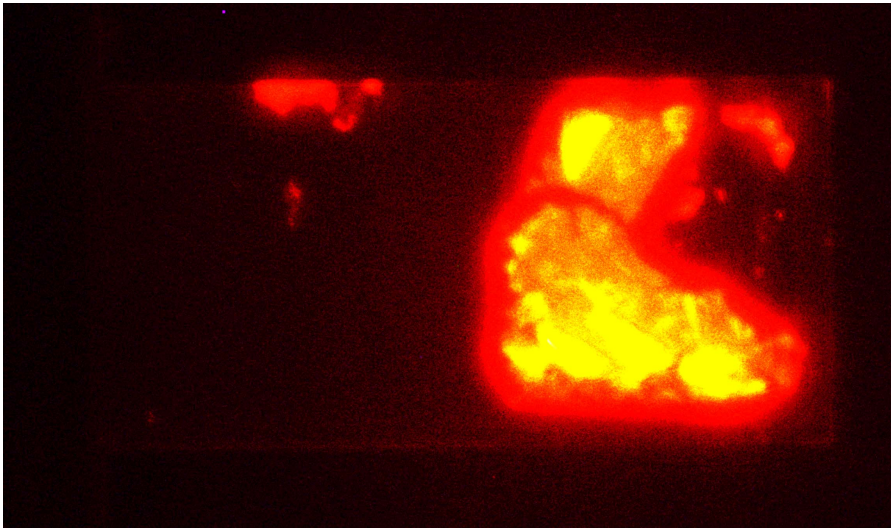


Figure 26: Fluorescence microscopy image of a Si_3N_4 cantilever after complementary DNA hybridization.

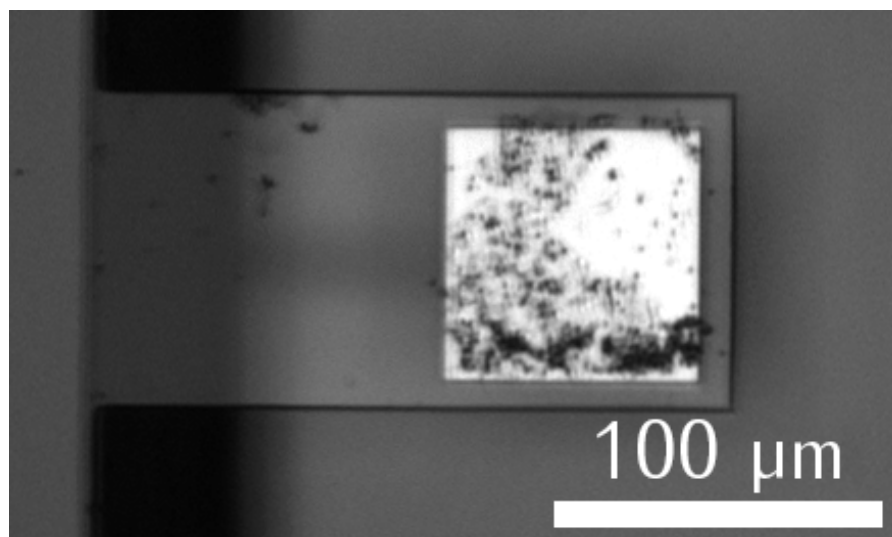


Figure 27: Debris on a Si₃N₄ cantilever. Greyscale image obtained with an optical microscope (10× magnification).

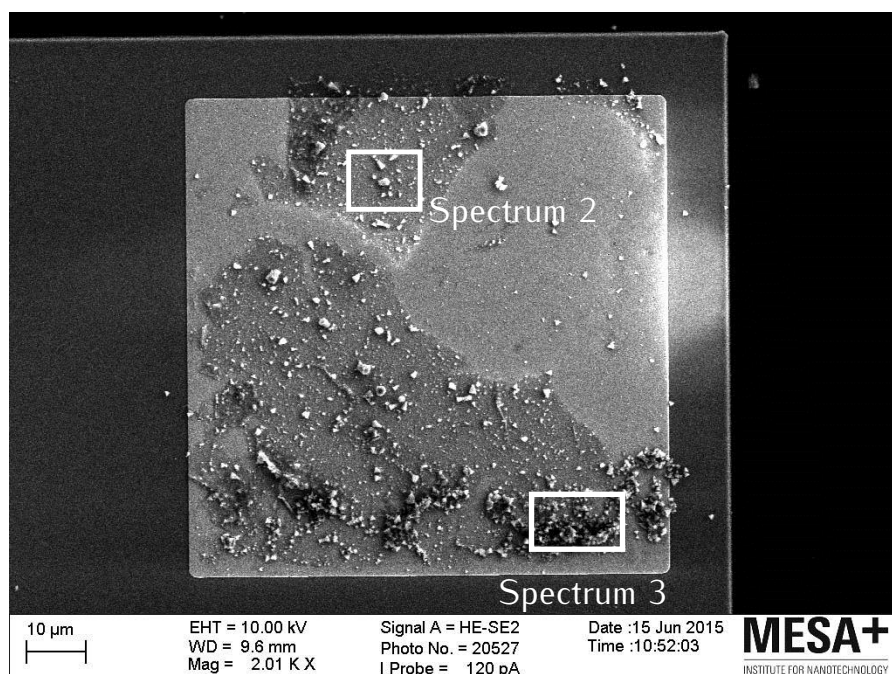


Figure 28: SEM micrograph of a Si₃N₄ cantilever after complementary DNA hybridization. White boxes indicate the positions on which EDS spectra are recorded (see figs. 29 and 30).

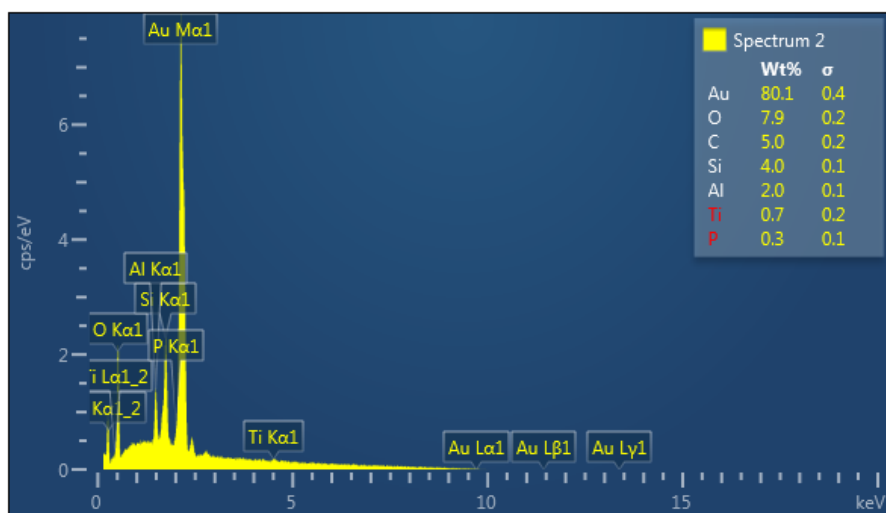


Figure 29: EDS spectrum (2) of debris on a Si_3N_4 cantilever after complementary DNA hybridization. The position where this spectrum is taken is indicated in fig. 28.

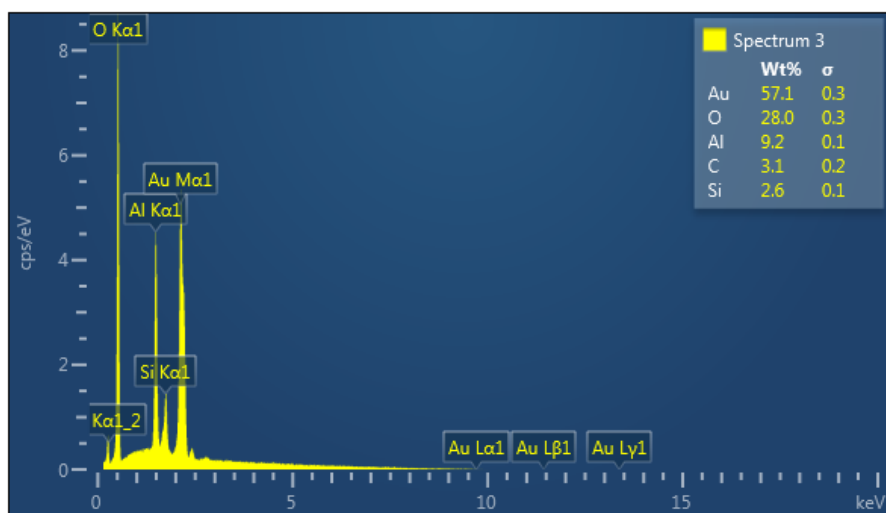


Figure 30: EDS spectrum (3) micrograph of a Si_3N_4 cantilever after complementary DNA hybridization. The position where this spectrum is taken is indicated in fig. 28.

A.6 CHALLENGES

Unpublished work by Harmen Koster recently showed fluorescence microscopy images which indicate that the PZT layer of the previous generation of micro-cantilevers in the *Nanopill 2.0* project is not fully covered by silicon oxide. The uncovered PZT attracts DNA, probably due to electrostatic forces. SEM-EDX confirms the presence of uncovered PZT surfaces (fig. 31). No fluorescence is observed on the gold patches at the tip, which is consistent with the findings in this thesis, see e.g. fig. 33. Furthermore, the gold tips don't look shiny under an optical microscope as they should. Scanning electron microscopy reveals that the gold layer peels off from many cantilevers as shown in fig. 32. These challenges motivated the fabrication of the new devices which are studied in this thesis.

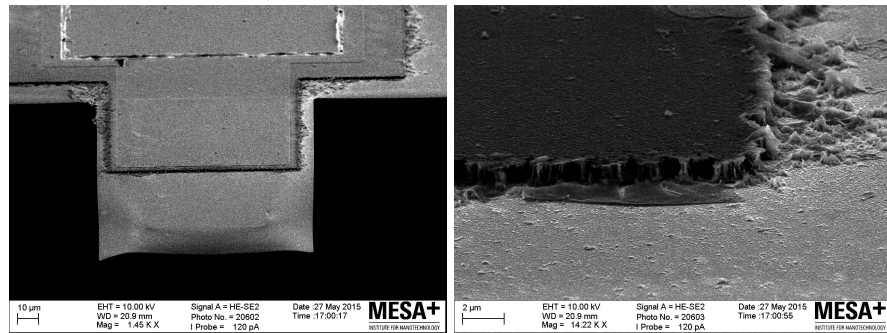


Figure 31: SEM micrographs of a silicon cantilever with partially uncovered PZT. Tilted view on cantilever and its associated bond pad (left) and close-up on platinum-PZT interface (right)

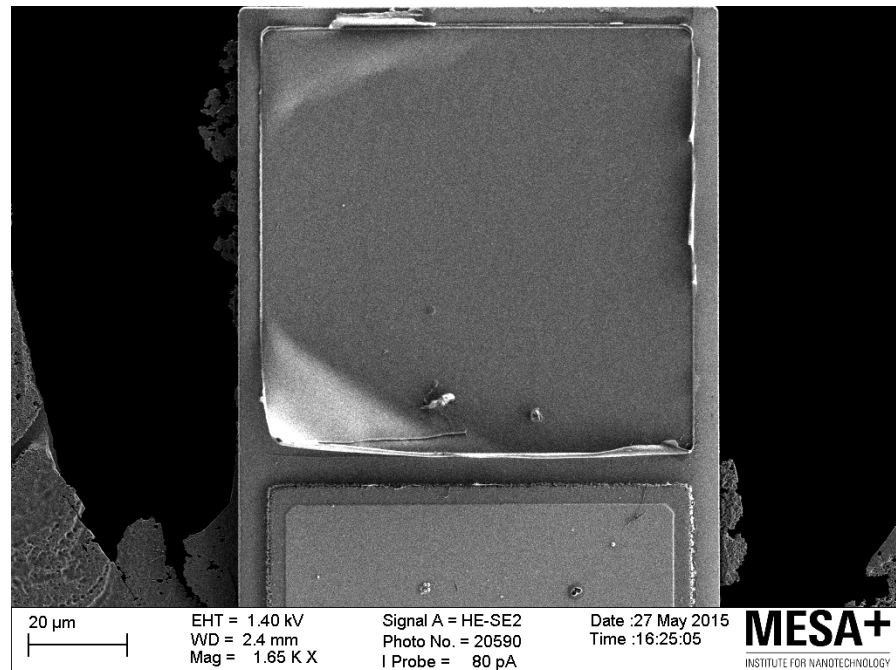


Figure 32: SEM micrograph of a cantilever where the gold is peeling off from the tip

A.7 ADDITIONAL FLUORESCENCE MICROSCOPY IMAGES

Figure 33 presents a comparison of two representative fluorescence microscopy images obtained in experimental round 3. For the control chip that was immersed in non-complementary DNA solution to be visible at all, the exposure time had to be chosen much larger as for the chip with complementary DNA.

Even at very long exposure times, there is no fluorescence intensity on the gold area on any of the cantilevers.

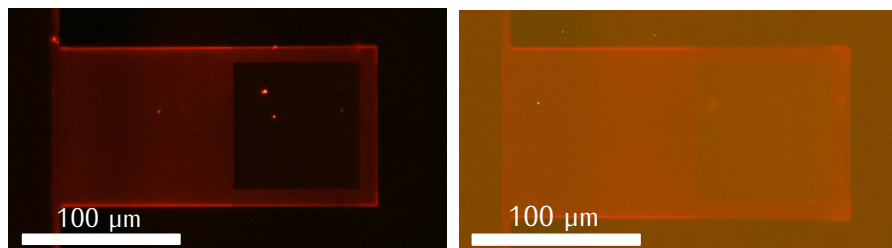


Figure 33: Comparison of fluorescence intensity in experimental round 3 between chip that was immersed in complementary DNA solution (left) for hybridization and non-complementary control (right). Camera exposure time 4.00 s (left) and 11.47 s (right).

A.8 ADDITIONAL XPS DATA

Figure 34 shows four additional XPS spectra with weak or no sulfur peaks. While the top left spectrum definitely exhibits a faint sulfur peak, the top right and bottom left spectra are more difficult to interpret but might still indicate the presence of a small amount of sulfur. These three spectra are recorded on gold coated cantilever tips and sulfur from the thiol-ssDNA is expected to be found there. The bottom right spectrum is taken on bare silicon nitride and therefore the absence of a sulphur peak is also expected. Table 5 shows the atomic concentration of carbon (C), nitrogen (N), oxygen (O), silicon (Si), phosphorus (P), sulfur (S), and gold (Au) at three different positions on each of the two cantilever chips analyzed by XPS.

This XPS data complements the results of experimental round 2 (see section 5.2)

Table 5: Overview of element concentration on the cantilevers used in round 2. Measurements are taken with XPS, the concentrations are given in at %. Sample names correspond with fig. 15, c and nc stand for cantilevers that were immersed in solution of complementary and non-complementary DNA during the hybridization step, respectively. Phosphorus (P) data seems reasonable but is not reliable in this experiment

Sample	C	N	O	Si	P	S	Au
c - w Au (A)	22.93	10.99	30.54	23.75	1.27	0.34	10.38
c - w/o Au (A)	18.21	25.41	22.46	33.07	0.65	0.00	0.21
c - w Au (B)	28.28	11.64	25.00	21.69	1.07	0.46	11.65
nc - w Au (A)	26.79	10.89	28.21	14.88	1.44	0.20	17.59
nc - w Au (B)	27.10	9.23	25.79	22.14	0.92	0.64	14.18
nc - w/o Au (D)	14.91	26.64	26.44	31.01	0.78	0.00	0.22

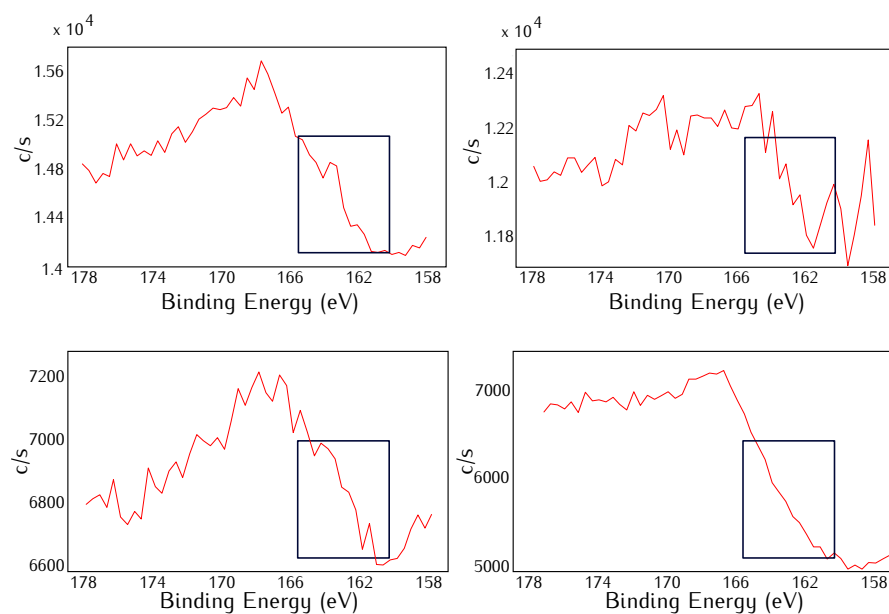


Figure 34: Additional XPS data: Upper spectra and bottom left are recorded on gold areas and interpreted to show faint indications for sulfur, bottom right spectrum is taken on bare silicon nitride for control and has no sulfur peak

BIBLIOGRAPHY

- Adjémian, J., A. Anne, G. Cauet, and C. Demaille
2010 "Cleavage-Sensing Redox Peptide Monolayers for the Rapid Measurement of the Proteolytic Activity of Trypsin and alpha-Thrombin Enzymes," *Langmuir*, vol. 26, 12, pp. 10347-10356, DOI: [10.1021/la100397g](https://doi.org/10.1021/la100397g).
- Álvarez, M., L. G. Carrascosa, M. Moreno, A. Calle, Á. Zaballos, L. M. Lechuga, C. Martínez-A, and J. Tamayo
2004 "Nanomechanics of the Formation of DNA Self-Assembled Monolayers and Hybridization on Microcantilevers," *Langmuir*, vol. 20, 22, pp. 9663-9668, DOI: [10.1021/la0489559](https://doi.org/10.1021/la0489559).
- Beck, M.
2013 "Should men get PSA tests to screen for prostate cancer?" *The Wall Street Journal*, vol. 2, p. 14.
- Carrascosa, L.G., M. Moreno, M. Álvarez, and L.M. Lechuga
2006 "Nanomechanical biosensors: a new sensing tool," *TrAC Trends in Analytical Chemistry*, vol. 25, 3, pp. 196-206, ISSN: 0165-9936, DOI: [10.1016/j.trac.2005.09.006](https://doi.org/10.1016/j.trac.2005.09.006).
- Cerruti, M., S. Fissolo, C. Carraro, C. Ricciardi, A. Majumdar, and R. Maboudian
2008 "Poly(ethylene glycol) Monolayer Formation and Stability on Gold and Silicon Nitride Substrates," *Langmuir*, vol. 24, 19, pp. 10646-10653, DOI: [10.1021/la801357v](https://doi.org/10.1021/la801357v).
- Chung, B.H., Y.-B. Shin, and M. Kim
2012 "Surface Plasmon Resonance," in *Encyclopedia of Cancer*, ed. by M. Schwab, Springer Berlin Heidelberg, pp. 3571-3574, ISBN: 978-3-642-16482-8, DOI: [10.1007/978-3-642-16483-5_5595](https://doi.org/10.1007/978-3-642-16483-5_5595).
- Delpu, Y., P. Cordelier, W.C. Cho, and J. Torrisani
2013 "DNA Methylation and Cancer Diagnosis," *International Journal of Molecular Sciences*, vol. 14, 7, pp. 15029-15058, ISSN: 1422-0067, DOI: [10.3390/ijms140715029](https://doi.org/10.3390/ijms140715029).
- Doínguez, C.M., P.M. Kosaka, G. Mokry, V. Pini, O. Malvar, M. del Rey, D. Ramos, Á. San Paulo, J. Tamayo, and M. Calleja
2014 "Hydration Induced Stress on DNA Monolayers Grafted on Microcantilevers," *Langmuir*, vol. 30, 36, pp. 10962-10969, DOI: [10.1021/la501865h](https://doi.org/10.1021/la501865h).
- Ebnesajjad, S.
2014 "Chapter 4 - Surface and Material Characterization Techniques," in *Surface Treatment of Materials for Adhesive Bonding*, ed. by S. Ebnesajjad, Second Edition, William Andrew Publishing, Oxford, pp. 39-75, DOI: [10.1016/B978-0-323-26435-8.00004-6](https://doi.org/10.1016/B978-0-323-26435-8.00004-6).

- Eom, K., H.S. Park, D.S. Yoon, and T. Kwon
2011 "Nanomechanical resonators and their applications in biological chemical detection: Nanomechanics principles," *Physics Reports*, vol. 503, 4-5, pp. 115-163, ISSN: 0370-1573, DOI: [10.1016/j.physrep.2011.03.002](https://doi.org/10.1016/j.physrep.2011.03.002).
- Esteller, M.
2007 "Cancer epigenomics: DNA methylomes and histone-modification maps," *Nat. Rev. Genet.*, vol. 8, 4, pp. 286-298, DOI: [10.1038/nrg2005](https://doi.org/10.1038/nrg2005).
- Ferrier, D.C., M.P. Shaver, and P.J.W. Hands
2015 "Micro- and nano-structure based oligonucleotide sensors," *Biosensors and Bioelectronics*, vol. 68, pp. 798-810, ISSN: 0956-5663, DOI: [10.1016/j.bios.2015.01.031](https://doi.org/10.1016/j.bios.2015.01.031).
- Fradet, Y.
2009 "Screening for bladder cancer: the best opportunity to reduce mortality," *Can Urol Assoc J*, vol. 3, 6 Suppl 4, pp. 180-183.
- Hagan, M.F. and A.K. Chakraborty
2004 "Hybridization dynamics of surface immobilized DNA," *The Journal of Chemical Physics*, vol. 120, 10, pp. 4958-4968, DOI: [10.1063/1.1645786](https://doi.org/10.1063/1.1645786).
- Henry, M. R., P. Wilkins Stevens, J. Sun, and D. M. Kelso
1999 "Real-time measurements of DNA hybridization on microparticles with fluorescence resonance energy transfer," *Anal. Biochem.*, vol. 276, 2, pp. 204-214, DOI: [10.1006/abio.1999.4344](https://doi.org/10.1006/abio.1999.4344).
- Herne, T.M. and M.J. Tarlov
1997 "Characterization of DNA Probes Immobilized on Gold Surfaces," *Journal of the American Chemical Society*, vol. 119, 38, pp. 8916-8920, DOI: [10.1021/ja9719586](https://doi.org/10.1021/ja9719586).
- Hoque, M.O., S. Begum, O. Topaloglu, A. Chatterjee, E. Rosenbaum, W. Van Criekinge, W.H. Westra, M. Schoenberg, M. Zahurak, S.N. Goodman, and D. Sidransky
2006 "Quantitation of Promoter Methylation of Multiple Genes in Urine DNA and Bladder Cancer Detection," *Journal of the National Cancer Institute*, vol. 98, 14, pp. 996-1004, DOI: [10.1093/jnci/djj265](https://doi.org/10.1093/jnci/djj265).
- Kandimalla, R., A.A. van Tilborg, and E.C. Zwarthoff
2013 "DNA methylation-based biomarkers in bladder cancer," *Nat Rev Urol*, vol. 10, 6, pp. 327-335, DOI: [10.1038/nrurol.2013.89](https://doi.org/10.1038/nrurol.2013.89).
- Keighley, S. D., P. Li, P. Estrela, and P. Migliorato
2008 "Optimization of {DNA} immobilization on gold electrodes for label-free detection by electrochemical impedance spectroscopy," *Biosensors and Bioelectronics*, vol. 23, 8, pp. 1291-1297, ISSN: 0956-5663, DOI: [10.1016/j.bios.2007.11.012](https://doi.org/10.1016/j.bios.2007.11.012).

- Kelly, J.D., T.J. Dudderidge, A. Wollenschlaeger, O. Okoturo, K. Burling, F. Tulloch, I. Halsall, T. Prevost, A.T. Prevost, J.C. Vasconcelos, W. Robson, H.Y. Leung, N. Vasev, R.S. Pickard, G.H. Williams, and K. Stoerber
- 2012 "Bladder Cancer Diagnosis and Identification of Clinically Significant Disease by Combined Urinary Detection of Mcm5 and Nuclear Matrix Protein 22," *PLoS ONE*, vol. 7, 7, DOI: [10.1371/journal.pone.0040305](https://doi.org/10.1371/journal.pone.0040305).
- Kosaka, P.M., J. Tamayo, J.J. Ruz, S. Puertas, E. Polo, V. Grazu, J.M. de la Fuente, and M. Calleja
- 2013 "Tackling reproducibility in microcantilever biosensors: a statistical approach for sensitive and specific end-point detection of immunoreactions," *Analyst*, vol. 138, pp. 863-872, DOI: [10.1039/C2AN36192B](https://doi.org/10.1039/C2AN36192B).
- LeBlond, L.
- 2012 *Nobody is perfect: Study shows people have 400 genetic flaws in DNA*, Accessed: 15.04.2015, <http://www.redorbit.com/news/health/1112744244/genetic-study-nobody-perfect-120712>.
- Li, Z., L. Zhang, S. Zeng, M. Zhang, E. Du, and B. Li
- 2014 "Effect of surface pretreatment on self-assembly of thiol-modified DNA monolayers on gold electrode," *Journal of Electroanalytical Chemistry*, vol. 722-723, pp. 131-140, ISSN: 1572-6657, DOI: [10.1016/j.jelechem.2014.03.035](https://doi.org/10.1016/j.jelechem.2014.03.035).
- Lokanathan, A.R., S. Zhang, V.R. Regina, M.A. Cole, R. Ogaki, M. Dong, F. Besenbacher, R.L. Meyer, and P. Kingshott
- 2011 "Mixed poly (ethylene glycol) and oligo (ethylene glycol) layers on gold as nonfouling surfaces created by backfilling," *Biointerphases*, vol. 6, 4, pp. 180-188, ISSN: 1934-8630, DOI: [10.1116/1.3647506](https://doi.org/10.1116/1.3647506).
- Looker, J.R. and J.E. Sader
- 2008 "Flexural resonant frequencies of thin rectangular cantilever plates," *Journal of Applied Mechanics*, vol. 75, 1, DOI: [10.1115/1.2745377](https://doi.org/10.1115/1.2745377).
- Magrab, E.B.
- 2012 *Vibrations of Elastic Systems - with applications to MEMS and NEMS*, Solid Mechanics and Its Applications, Springer Netherlands, vol. 184, DOI: [10.1007/978-94-007-2672-7](https://doi.org/10.1007/978-94-007-2672-7).
- McWilliams, A.
- 2013 "MEMS: Biosensors and Nanosensors," *BCC Research*.
- Mertens, J., C. Rogero, M. Calleja, D. Ramos, J. A. Martin-Gago, C. Briones, and J. Tamayo
- 2008 "Label-free detection of DNA hybridization based on hydration-induced tension in nucleic acid films," *Nat Nanotechnol*, vol. 3, 5, pp. 301-307.
- Ramos, D., M. Arroyo-Hernández, E. Gil-Santos, H. Duy Tong, C. Van Rijn, M. Calleja, and J. Tamayo
- 2009 "Arrays of Dual Nanomechanical Resonators for Selective Biological Detection," *Analytical Chemistry*, vol. 81, 6, pp. 2274-2279, DOI: [10.1021/ac8024152](https://doi.org/10.1021/ac8024152).

- Ravan, H., S. Kashanian, N. Sanadgol, A. Badoei-Dalfard, and Z. Karami
 2014 "Strategies for optimizing {DNA} hybridization on surfaces," *Analytical Biochemistry*, vol. 444, pp. 41-46, ISSN: 0003-2697, DOI: [10.1016/j.ab.2013.09.032](https://doi.org/10.1016/j.ab.2013.09.032).
- Reimhult, E. and F. Höök
 2015 "Design of Surface Modifications for Nanoscale Sensor Applications," *Sensors*, vol. 15, 1, p. 1635, ISSN: 1424-8220, DOI: [10.3390/s150101635](https://doi.org/10.3390/s150101635).
- Ron, H., S. Matlis, and I. Rubinstein
 1998 "Self-Assembled Monolayers on Oxidized Metals. 2. Gold Surface Oxidative Pretreatment, Monolayer Properties, and Depression Formation," *Langmuir*, vol. 14, 5, pp. 1116-1121, DOI: [10.1021/la970785v](https://doi.org/10.1021/la970785v).
- Ruz, J. J., J. Tamayo, V. Pini, P. M. Kosaka, and M. Calleja
 2014 "Physics of nanomechanical spectrometry of viruses," *Sci Rep*, vol. 4, DOI: [10.1038/srep06051](https://doi.org/10.1038/srep06051).
- Senturia, S.D.
 2001 *Microsystem Design*, Springer US, ISBN: 9780792372462, DOI: [10.1007/b117574](https://doi.org/10.1007/b117574).
- Shen, F., P. Lu, S.J. O'Shea, K.H. Lee, and T.Y. Ng
 2001 "Thermal effects on coated resonant microcantilevers," *Sensors and Actuators A: Physical*, vol. 95, 1, pp. 17-23, ISSN: 0924-4247, DOI: [10.1016/S0924-4247\(01\)00715-4](https://doi.org/10.1016/S0924-4247(01)00715-4).
- Sievert, K. D., B. Amend, U. Nagele, D. Schilling, J. Bedke, M. Horstmann, J. Hennenlotter, S. Kruck, and A. Stenzl
 2009 "Economic aspects of bladder cancer: what are the benefits and costs?" *World J Urol*, vol. 27, 3, pp. 295-300, DOI: [10.1007/s00345-009-0395-z](https://doi.org/10.1007/s00345-009-0395-z).
- Steel, A. B., R. L. Levicky, T. M. Herne, and M. J. Tarlov
 2000 "Immobilization of nucleic acids at solid surfaces: effect of oligonucleotide length on layer assembly," *Biophys. J.*, vol. 79, 2, pp. 975-981.
- Strømmen, E.N.
 2014 *Structural Dynamics*, Springer Series in Solid and Structural Mechanics, Springer International Publishing, vol. 2, DOI: [10.1007/978-3-319-01802-7](https://doi.org/10.1007/978-3-319-01802-7).
- Svatek, R. S., B. K. Hollenbeck, S. Holmang, R. Lee, S. P. Kim, A. Stenzl, and Y. Lotan
 2014 "The economics of bladder cancer: costs and considerations of caring for this disease," *Eur. Urol.*, vol. 66, 2, pp. 253-262, DOI: [10.1016/j.eururo.2014.01.006](https://doi.org/10.1016/j.eururo.2014.01.006).
- Tamayo, J., P.M. Kosaka, J.J. Ruz, A. San Paulo, and M. Calleja
 2013 "Biosensors based on nanomechanical systems," *Chem. Soc. Rev.*, vol. 42, pp. 1287-1311, DOI: [10.1039/C2CS35293A](https://doi.org/10.1039/C2CS35293A).

- Vidyasekar, P., P. Shyamsunder, and R.S. Verma
 2012 "Chapter 7 - Nanobiotechnology: A New Generation of Biomedicine - Innovative Nanotechnology in Key Areas of Biomedical Engineering and Cancer Therapy," in *Nanotechnology in Health Care*, ed. by S.K. Sahoo, First Edition, Pan Stanford Publishing, pp. 237-273, DOI: [10.1201/b13159-8](https://doi.org/10.1201/b13159-8).
- Waggoner, P.S., M. Varshney, and H.G. Craighead
 2009 "Detection of prostate specific antigen with nanomechanical resonators," *Lab Chip*, vol. 9, pp. 3095-3099, DOI: [10.1039/B907309B](https://doi.org/10.1039/B907309B).
- Wernette, D. P., C. Mead, P.W. Bohn, and Y. Lu
 2007 "Surface Immobilization of Catalytic Beacons Based on Ratiometric Fluorescent DNAzyme Sensors: A Systematic Study," *Langmuir*, vol. 23, 18, pp. 9513-9521, DOI: [10.1021/la701303k](https://doi.org/10.1021/la701303k).
- Xu, X. and Z. Deng
 2013 "Surface effects of adsorption-induced resonance analysis on micro/nanobeams via nonlocal elasticity," *Applied Mathematics and Mechanics*, vol. 34, 1, pp. 37-44, ISSN: 0253-4827, DOI: [10.1007/s10483-013-1651-9](https://doi.org/10.1007/s10483-013-1651-9).
- Xue, Y., Y. Chen, Q. Ayub, N. Huang, E.V. Ball, M. Mort, A.D. Phillips, K. Shaw, P.D. Stenson, D.N. Cooper, and C. Tyler-Smith
 2012 "Deleterious- and Disease-Allele Prevalence in Healthy Individuals: Insights from Current Predictions, Mutation Databases, and Population-Scale Resequencing," *The American Journal of Human Genetics*, vol. 91, 6, pp. 1022-1032, ISSN: 0002-9297, DOI: [10.1016/j.ajhg.2012.10.015](https://doi.org/10.1016/j.ajhg.2012.10.015).
- Xylinas, E., L. A. Kluth, M. Rieken, P. I. Karakiewicz, Y. Lotan, and S. F. Shariat
 2014 "Urine markers for detection and surveillance of bladder cancer," *Urol. Oncol.*, vol. 32, 3, pp. 222-229.
- Yang, F.
 2012 "Effect of Surface Viscosity on the Vibration of Microcantilevers," *Langmuir*, vol. 28, 7, pp. 3449-3452, DOI: [10.1021/la204235f](https://doi.org/10.1021/la204235f).
- Yu, Y., S. Blair, D. Gillespie, R. Jensen, D. Myszka, A. H. Badran, I. Ghosh, and A. Chagovetz
 2010 "Direct DNA methylation profiling using methyl binding domain proteins," *Anal. Chem.*, vol. 82, 12, pp. 5012-5019, DOI: [10.1021/ac1010316](https://doi.org/10.1021/ac1010316).